UNIVERSITY OF CALIFORNIA,
IRVINE

Seismic Performance Simulation of Magnetorheological Fluid Dampers with Single Degree-of-Freedom System

THESIS

submitted in partial satisfaction of the requirements.
for the degree of

MASTER OF SCIENCE

in Civil Engineering

by

Yuan Gao

Thesis Committee:
Professor Lizhi Sun, Chair
Associate Professor Mo Li
Assistant Professor Joel Lanning

2021

DEDICATION

To my parents for your understanding and encouragement to my every idea, and the people who accompany me, and support me all the time.

TABLE OF CONTENTS

LIST OF FIGURES

LIST OF TABLES

ACKNOWLEDGEMENTS

I would like to express the deepest thanks to my advisor, Professor Lizhi Sun, for his inestimable support, encouragement, and guidance throughout the completion of this thesis.

I would like to express my gratitude to the committee members, Professor Mo Li and Professor Joel Lanning.

I would like to thank my family and friends for their unconditional support.

ABSTRACT OF THE THESIS

Seismic Performance Simulation of Magnetorheological Fluid Dampers with Single Degree-of-Freedom System

by

Yuan Gao
Master of Science in Civil Engineering
University of California, Irvine, 2021

Professor Lizhi Sun, Chair

After the 1994 Northridge earthquake, to prevent the existing buildings from brittle damage and failure at the beam-column connections, a variety of energy dissipation devices have been developed. The magnetorheological (MR) fluid dampers stand out for their endurance, instant response, and adjustable damping force, etc. This study evaluates the seismic performances of the MR dampers applied with the Bouc-Wen model (MR-BW) and BWBN model (MR-BWBN), respectively, via comparing with a conventional viscoelastic damper model (VE) under the ground motions with three different peak ground acceleration (PGA) levels. The damper systems along with a moment-resisting frame (MF) simplified as SDOF system were modeled, and modal, pushover, harmonic, and transient analyses were performed using the finite element method. The results show that the natural frequency of an MF will be increased with the application of damper systems. Under the same transverse loading, the MR-BWBN may reduce more plastic deformation than the MR-BW and VE. Additionally, the maximum drift ratios of MR-BWBN were lower than the others subjected to PGA $= 0.4$ g and PGA $= 0.588$ g earthquakes, respectively. The cumulative energy dissipated by MR-BWBN is less than MR-BW subjected to the PGA $= 0.2$ g earthquake, but more under the PGA $= 0.4$ g and PGA $= 0.588$ g earthquakes.

Chapter 1. Introduction

1.1. Northridge Earthquake

Earthquakes are catastrophic events that occur mostly at the boundaries of portions of the Earth's crust called tectonic plates [1]. On 17th January, an M_w 6.7 earthquake struck Northridge, California. The fault leading to the Northridge earthquake is part of a broad system of thrust faults at the Big Bend of the San Andreas fault, originating from the left step in the Pacific-North American plate Boundary [2]. The Northridge earthquake caused the greatest damage in the United States since the 1906 San Francisco earthquake [3]. The death toll was 57 and more than 8,700 people were injured, approximately 12500 structures were damaged in varying degrees, leaving thousands of people temporarily homeless. The property damage of an estimated $13-50 billion due to the Northridge earthquake making it one of the costliest natural disasters in U.S. history [4]. More than 150 damaged buildings, including hospitals and other health care facilities, government, civil and private offices, cultural and educational facilities, residential structures, and commercial and industrial buildings, have been identified after the Northridge earthquake [5].

To investigate the causations of failure of structures, the SAC Steel Project, sponsored by the Federal Emergency Management Agency (FEMA), collaborated with three major Associations- Structural Engineers Association of California (SEAC), Applied Technology Council (ATC), and Consortium of Universities for Research in Earthquake Engineering (CUREE) to research the structural failures and suggest preventive measures retrofitting existing buildings. It is concluded that the main structural damage resulted

from the failures of the moment-resisting beam-column connections including beam-column flange fractures, column web, and panel zone fractures. The results of these studies in the SAC Phase II project have been published in FEMA 350. The use of energy dissipation or damping systems was regarded as a new technology by structural engineers, for the retrofit of vulnerable moment-frame buildings was not considered in the SAC Phase II project and prompted the study presented in this paper [6,7].

1.2. Seismic Retrofit

Seismic retrofitting is to modify existing structures to make them more resistant to seismic activity, ground motion, or soil failure due to earthquakes. It begins to attract more and more attention in recent years because some old buildings that were built many years ago need to be reinforced to meet the requirements of the present building codes. Some retrofitting programs are even mandatory such as the Soft-Story Retrofit Program supervised by the Los Angeles Department of Building and Safety (LA-DBS) under Ordinance 183893 and Ordinance 184081 [8,9].

The technique of the seismic renovation includes external post-tensioning [10], additional shear walls, supplementary dampers system, base isolators, etc. The application of the damper system enables the retrofitting process to be time-saving, high effectiveness, and less space to be taken. For example, in the seismic retrofitting project of Robert A. Young (RAY) Federal Building, damper systems were accepted as one of the solutions for seismic renovation. Because the dampers are made from steel frames, the open space within the structural elements is utilized to place the mechanical systems, so both were concealed from view within architectural partition walls, which is one of the advantages over solid concrete shear walls. Another advantage is the convenience of installation of dampers could cut down construction time and space occupation

during construction, thereby reducing the inconvenience for the people working there [11].

1.3. Energy Dissipation Systems in Structure

Damping or energy dissipation devices incorporated into new or existing buildings are to dissipate much or all the earthquake-induced energy in disposable elements that do not form part of the gravity framing system [6,7]. An idealized structure of figure 1 will be analyzed to illustrate the effect of adding energy dissipation systems in structures when subjected to a single historical earthquake record. A damage measure (DM) is built by Symans et al (2008) to quantify the damage in the frame. Damage measure equation is given by:

$$DM = \frac{\mu_{Demand}}{\mu_{Capacity}} + 4\rho \frac{E_{Demand}}{E_{Capacity}} \quad (1)$$

Where μ_{Demand} and E_{Demand} are maximum displacement ductility demand and cumulative hysteretic energy dissipation demand respectively in the system; $\mu_{Capacity}$ and $E_{Capacity}$ are ductility capacity and hysteretic energy capacity respectively for on full cycle of inelastic deformation of the system. ρ is calibration factor that is material dependent and used for producing a DM value range from 0~1. DM value is 0.0 when the structures are undamaged, and 1.0 when the damage is severe (near or at the initial collapse). Eq. (1) is typically applied to a

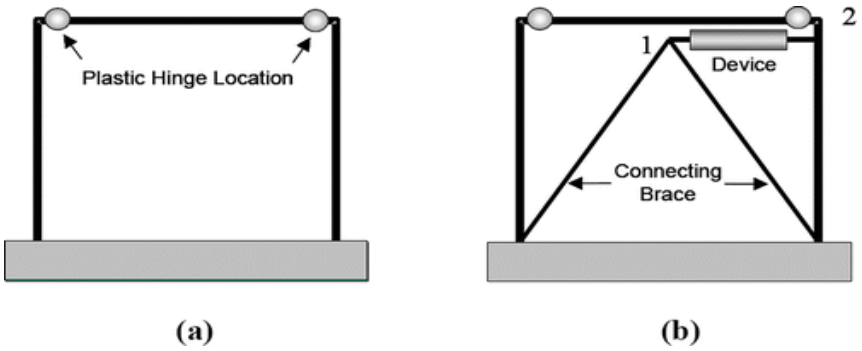

Figure 1. Frame without and with passive energy dissipation devices [12]

critical element or component of a structure instead of to the whole structure [12]. In the example shown in figure 1, Eq. (1) applied to the simplified system. An energy balance equation is given by Uang and Bertero (1999):

$$E_I = E_S + E_K + E_D + E_H \tag{2}$$

where at the time t, E_I is cumulative input energy; E_S is instantaneous strain energy stored by the structure; E_K is instantaneous kinetic energy of the moving mass; E_D is cumulative viscous damping energy; E_H is cumulative hysteretic energy. In this example, the energy dissipation demand in Eq. (1) is equal to the cumulative hysteretic energy dissipated by the formation of plastic hinges in the girders. At the end of the seismic vibration, E_K and E_S are both zero for the elastic system while near zero for the inelastic system. Under the circumstance of no external energy dissipation devices added to the system, E_H at the end of the earthquake is equal to the energy demand. Decreasing μ_{Demand} and E_{Demand} or increasing the $\mu_{Capacity}$ and $E_{Capacity}$ can reduce the structural damage as indicated in Eq. (1). In other words, reducing the damage of structure can be considered from the aspect of decreasing the ductility or hysteretic energy demand or by increasing the ductility or hysteretic energy capacity. The increasing ductility or hysteretic energy capacity sets higher demand for material properties and is not recognized to be economic. Therefore, reducing the ductility or the energy dissipation demand may improve the performance of structures feasibly. Hence, adding energy dissipation devices such as damper systems was considered as one of the methods to reduce the ductility and hysteretic energy dissipation effectively [13].

1.4. Control Systems for Seismic Protection of Structures

Symans and Constantinous (1999) summarized the development of Semi-active control systems for seismic protection of structures and stated that the control systems for seismic protection of structures can be defined as three major classes: Passive control systems, Active control systems, and Semi-active control systems. A passive control system utilized the motion of the structures to develop the control forces without the requirement of an external power source, as showed in figure 2(a). It is a traditional approach to mitigate seismic hazards through sufficient strength capacity and ductile deformation. Such systems were referred to as supplemental energy dissipation systems that take many forms and dissipate energy through various mechanisms including metallic yielding, sliding friction, and viscous fluid, etc., which are represented by structural bracing, friction damper, and viscous fluid damper, respectively [14,15]. However, passive systems are unable to adapt to changes in the structural properties under random external excitation such as earthquake activities, which leads to a new research direction that utilizing the external forces to overcome the deficiency of passive control system [16].

Contrary to the passive control systems, an active control system requires a large power source for operating electrohydraulic or electromechanical actuators that provide extra control forces to the structure [see figure 2(b)]. Control forces are activated by the feedback from sensors implanted in the structures that measure the excitation, based on a pre-determined control algorithm. However, the Active control system may encounter reliability issues resulted from significant and variable input time delay resulted because the actual time delay also depends on the input time increment value at each sampling point [17].

Semi-active control systems achieve a comprise between passive and active control

systems. Maintaining the inherent reliability of passive control systems while taking the advantage of the adaptability of active systems without requiring significant external power is a unique advantage of the semi-active control system. In addition, Semi-active control systems can promote the global stability system because the control forces were primarily acted to oppose the motion of the structural system. Semi-active control systems also are more environmentally friendly for requiring a small amount of external power that is on the order of tens of watts, comparing with active control systems that the external power on the order of tens of kilowatts is required [15]. Stiffness control devices such as adaptive tuned mass dampers and semi-active tuned mass dampers have been equipped within a large variety of buildings to reduce the dynamic response [18]. Besides, magnetorheological fluid (MRF) damper is also a type of semi-active damper and was a recognized example of the smart dampers among semi-active devices [19].

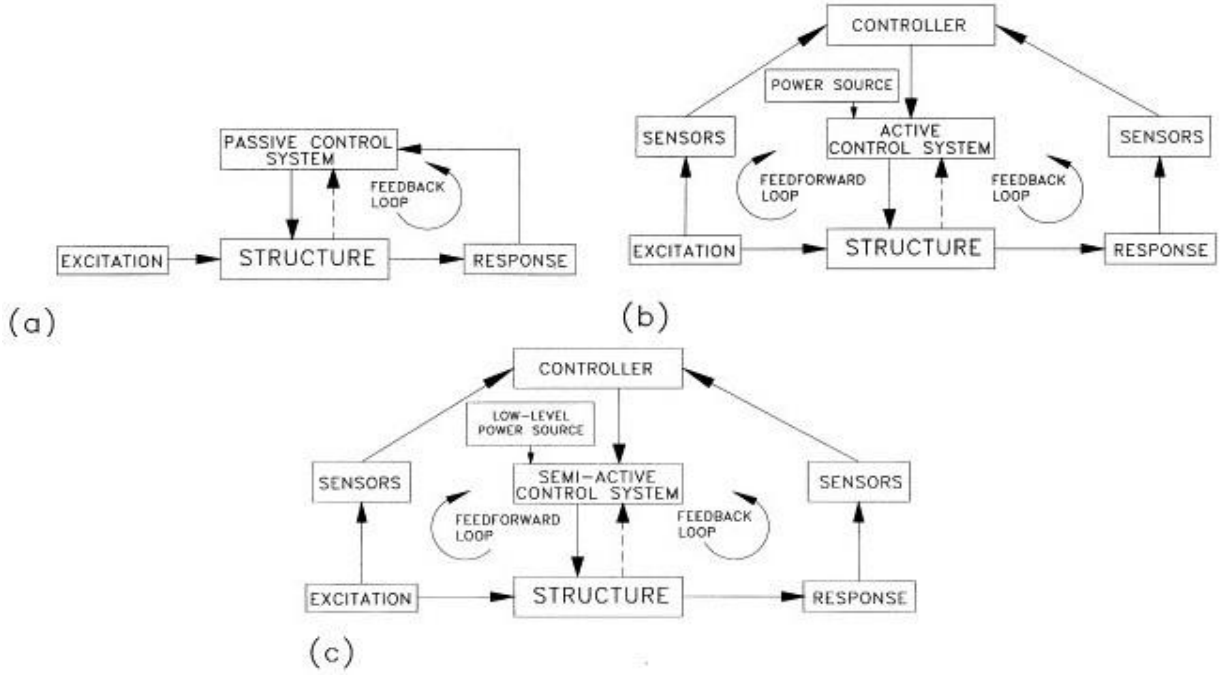

Figure 2. Block Diagram of Structural Control Systems: (a) Passive Control System; (b) Active Control System; (c) Semi-Active Control System [15].

Chapter 2. MRF Dampers

2.1. MR Materials

MR material is one of the branches of smart materials for their significant rheological characteristics when subjected to external magnetic fields, and its original properties can be recovered within a millisecond after the external field is removed. Jacob Rabinow discovered MR fluid and developed a clutch for vehicles at the US National Bureau of Standards in 1948 [19]. Since then, the Electrorheological (ER) fluid attract more attention in most research than MR fluid, which was invented almost the same time as MR fluid, for it has shown broad potential in many application such as fast-acting hydraulic valves, clutches, shock absorbers, accurate abrasive polishing, haptic controllers and so on, although so disadvantages were exposed including low yield strength, sensitivity to general contaminants, high voltage demanding, narrow working temperature range, etc. Hence, some researchers turned to study MR fluid since the 1990s, because it showed better performance than ER fluid in the aspects mentioned above, for instance, higher yield strength by one order of magnitude, insensitivity to contaminants, 12-24 V low voltage demanding, and so on [20].

Jolly et al (1996) defined that "magnetorheological (MR) materials consist of micro-size (typically three to five microns) magnetically permeable particles suspended in a non-magnetic medium". According to this definition, MR materials that were applied in practice mostly take the forms of MR fluid or MR elastomer (MREs). The main difference between the MR fluid damper and MR elastomer is the materials of the carrier medium. For MR fluid dampers, the carrier medium may take the physical form of liquid, such as mineral or silicone oil, while for

MR elastomer, various types of rubber are the common matrix for MR elastomer researched as vibration isolator located at the bottom of the buildings [21], [22].

Due to its ability to adapt rheological properties quickly under various degrees of magnetic fields, the MR material has gained significant attention as a smart material [23]. In the civil engineering field, MR dampers were used to mitigate the dynamic response of the structures by shock absorption resulted from earthquake activities or strong wind, cable-stayed bridges. A prototype MR damper was described by Spencer et al and Dyke et al. Shaking table test also performed by Dyke et al on reduced-scale structure for testing the seismic response. Subsequently, Spencer et al and Carlson developed and tested a large-scale MR damper for seismic response control [24-27].

2.2. Properties of MR Fluid Dampers

MR Fluid is one of the members of the smart material family, which consists of liquid carrier medium, ferromagnetic particles (typically iron), and a variety of additives like grease or some thixotropic additive to improve settling stability. Before the application of magnetic field, the MR fluid is in the physical form of a Newtonian fluid, however, the MR

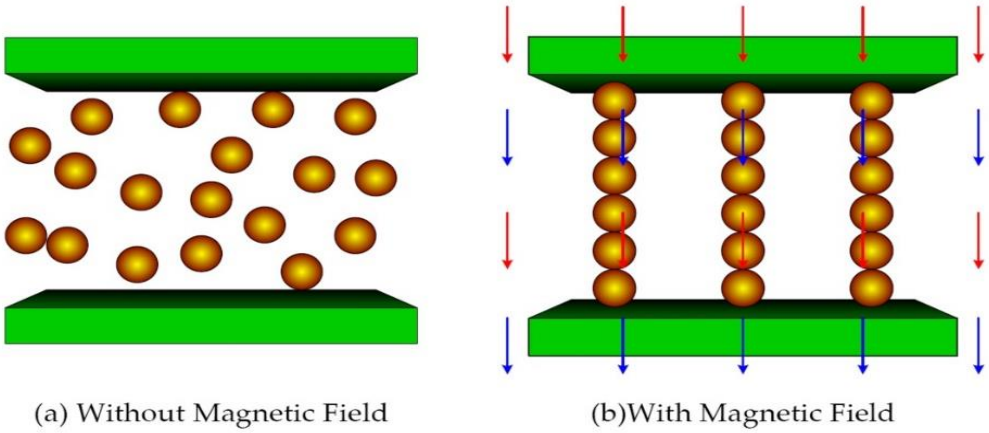

Figure 3. MR Fluid– Working Principle [32]

fluid change from Newtonian fluid to semi-solid state when the external magnetic field was applied and recover to the original state instantly after removal of the magnetic field. The most remarkable feature is that such alternation just happened in millisecond, and it means the yield strength of MR fluid is instantly controllable when exposed to magnetic field [28]. The microscopic mechanism responsible for this phenomenon is the induced magnetic mutual interaction of particles within the matrix, which instantly transforms the ferromagnetic particles in the MR fluid from a disordered state into chain-like structures that the particles were aligned roughly parallel to the magnetic field [see figure 3]. Therefore, MR dampers can generate different damping forces and cause changeable structural stiffness under various external currents [29], [30].

Yield strength is one of the indexes to measure the performance of MR Fluid damper in practice. In 1948, to estimate the maximum yield strength of MR fluid, Rabinow suspended a young woman into air utilizing a simple direct shear MR fluid device, the MR fluid inside consisted of 9 parts by weight of carbonyl iron to one part of silicone oil and grease or thixotropic additive, the total shear area is 8 in^2, and the weight of the woman is 117lb. This simple experiment demonstrated that the MR fluid has at least 100kPa of yield strength [31], [32]. The subsequent research indicated the yield strength of MR fluid varies from different flow modes.

MR fluids have three distinct modes of operation and applications, as shown in figure 5. In valve mode, MR fluid flowing resulted from a pressure difference perpendicular to the magnetic field line, and magnetic poles are fixed [see figure 5 (a)]. The direct shear mode works as its name implied, MR fluid is being sheared and one of the poles is moving relative to the other pole [see figure 4 (b)]. Comparing to shear and valve modes, the

squeeze mode can generate a much larger range of damping force in small operational envelopes [see figure 4 (c)]. Hong-yun et al stated that the SG MRF2053 has a maximum yield stress of 53kPa without compression process. However, the maximum yield stress of it can exceed 1100kPa when the applied current is 2.5A along with 2.0 MPa compressive stress. [33], [34]. In addition to the three main modes, the shear-valve mode was proposed as a combination of shear mode and valve mode [see figure 5]. Due to the high efficiency and geometry simplicity, the shear-valve model has been employed extensively in the civil engineering field [35], [36].

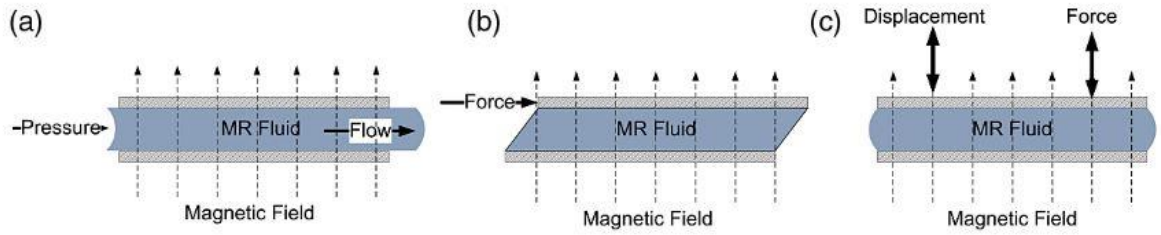

Figure 4. MR Fluid Flow Modes [34]

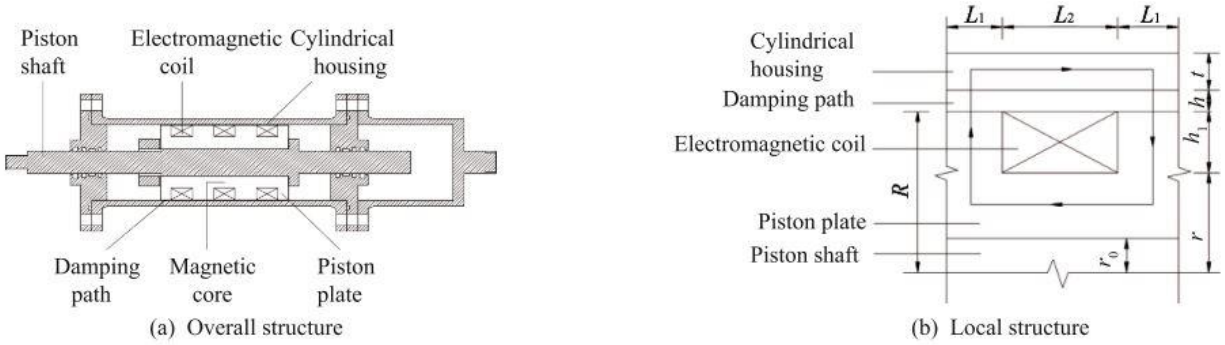

Figure 5. Schematic Diagram of a Shear-valve MR Damper [36]

2.3. Modeling of MRF Dampers

2.3.1. Bingham Model

The Bingham model, due to its simplicity, is frequently used to characterize the dynamic behavior of MR dampers. The model is composed of a dashpot and a friction element connected in parallel [see figure 6(a)]. The restoring force in the Bingham is given by:

$$F = c_1\dot{x} + f_0 sgn(\dot{x}) \tag{3}$$

where x is the damper displacement, c_1 is the damping coefficient, f_0 represents the slider friction force [37]. Eq. (3) shows the damping force is linearly dependent on the damper velocity, the friction force is decided by the sign of the velocity. The Bingham model can predict the force-displacement relationship for MR dampers while cannot describe the force-velocity relationship, as it has only one path in the force-velocity plot, as shown in figure 6 [38].

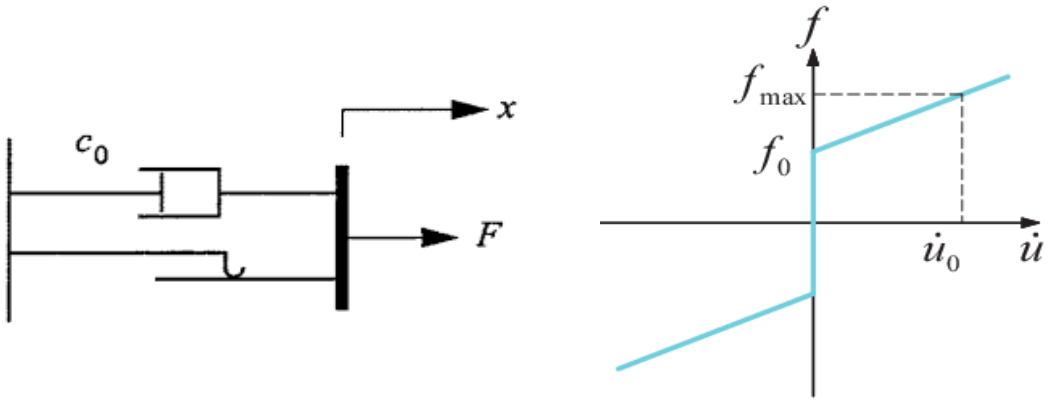

(a) (b)

Figure 6. Bingham Model: (a) Schematic Model [37]; (b) Force-Velocity Curve [38]

2.3.2. Gamota and Filisko Model

Gamota and Filisko model was originally developed to describe the behavior of Electrorheological (ER) materials, but later, it was applied to the modeling of MR damper as well. The so-called Gamota and Filisko model is an extension of the Bingham model which is connected in series with a parallel set of spring and viscous damper [see figure 7]. The governing equations for this modified Bingham model are expressed as follows:

$$\left.\begin{aligned} F &= k_1(x_2 - x_1) + c_1(\dot{x}_2 - \dot{x}_1) + f_0 \\ &= c_0\dot{x}_1 + f_c\, sgn(\dot{x}_1) + f_0 \\ &= k_2(x_3 - x_2) + f_0 \end{aligned}\right\} if\ |f| > f_c \tag{4}$$

$$\left.\begin{aligned} F &= k_1(x_2 - x_1) + c_1(\dot{x}_2 - \dot{x}_1) + f_0 \\ &= k_2(x_3 - x_2) + f_0 \end{aligned}\right\} if\ |f| > f_c \tag{5}$$

Comparing with the Bingham model, Gamota and Filisko model can describe the hysteresis loop of MR damper more accurately, however, the simulation of it requires step size in the order of 10^{-6}, which take a long time and a huge computational work [26].

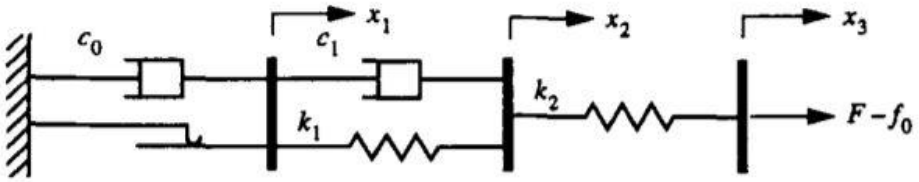

Figure 7. Gamota and Filisko Model [26].

2.3.3. Bouc-Wen Model

Due to the extreme versatility, the Bouc-Wen model can exhibit a wide variety of hysteretic behavior. A schematic Bouc-Wen model is shown in figure 8. The damper force is given by:

$$F = c_0\dot{u}(t) + k_0(u(t) - u_0) + \alpha z(t) \tag{6}$$

$$\dot{z}(t) = -\gamma|\dot{u}(t)|z(t)|z(t)|^{n-1} - \beta\dot{u}(t)|z(t)|^{n} + A\dot{u}(t) \quad (7)$$

where α is the ratio of post-yield stiffness to elastic stiffness, k_0 represents the elastic stiffness, The linearity in the unloading and the smoothness of transition from the pre-yield to the postyield region can be controlled by adjusting the parameters γ, β, A of the model. n is also a characteristic parameter like γ, β, and A. In addition, the force f_0 from the accumulator can be incorporated as an initial deflection x_0 of the elastic spring k_0 [26].

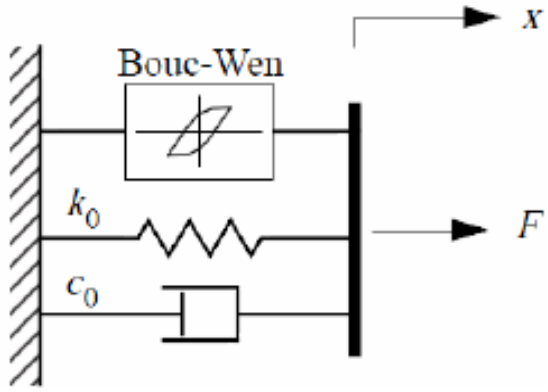

Figure 8. Bouc-Wen Model of MR damper [26]

Chapter 3. Methodology

3.1. Modeling of Moment-Resisting Frames

As mentioned in the beginning of this paper, to improve the capability of reducing the seismic response of old buildings, a series of preventive retrofitting measures have be done for existing buildings. Due to the widespread adoption of steel moment frames in commercial buildings, a single-story steel moment frame (MF) is selected as a carrier for analyzing the performance of the MR fluid damper. The Open System for earthquake engineering simulation (OpenSees) was applied through all the simulation processes mentioned in this paper. It is an open-source framework for the simulation of structural seismic response and geotechnical systems via finite element method (FEM). Because of the flexibility that allows the developers to create their own material or elements using the TCL programming language, low requirements of computer configuration, and timesaving, etc., OpenSees become more and more popular in the field of civil engineering.

Figure 9 (a) shows the sketch of a single-story steel MF made up of two W12 × 106 columns and one W12 × 87 beam. The steel type is ASTM A36 with an expected yield strength of 250 MPa. The model is two-dimensional, so the connections of column-foundation are rigid

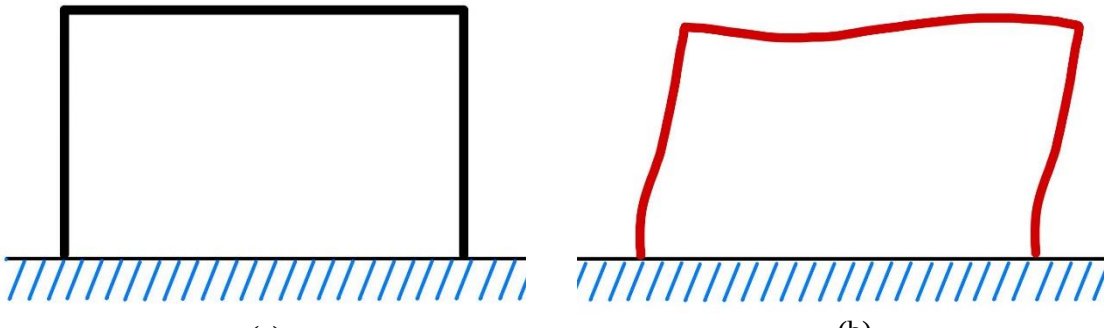

(a) (b)

Figure 9. Sketch of Single-Story MF

which means they are fully restrained, meanwhile, the column-beam connections are locked on the translation of the z-axis and the rotation about the x and y-axis. During horizontal ground motion, bending occurred near the end of beams and columns due to steel yielding as shown in figure 9 (b). If the connections are stronger than the connected members, column-beam and column-foundation connections can remain 90° and the plastic hinges will be in the members before connection failure. The structural properties of MF shown in figure 9 are listed in Table 1. The mass of the structure was assumed as lumped at the beam level and the beam with infinite axial stiffness. Hence, the MF herein can be considered as a single-degree-of-freedom (SDOF) system [39].

Table 1. Structural Properties of MF

Length of the beam (distance between column centerlines)	6000 mm
Height of column	3600 mm
Beam	W 12 × 87
Column	W 12 × 106
Expected yield strength (ASTM A36)	250 MPa (36 ksi)
Lumped mass	78400 kg
Moment of inertia of column cross-section	308011255 mm^4
Moment of inertia of beam cross-section	388343920 mm^4
Plastic moment capacity of columns	667 kN.m
Plastic moment capacity of the beam	537 kN.m

The modeling of MF in OpenSees is two-dimensional, so there are only three degrees of freedom for each node, the translation along the x and y-axis as well as the rotation about the z-axis. The MF was composed of four nodes and three elements as shown in figure 10, node 1 and node 4 are both fixed to ground for all three degrees of freedom which represent the column-foundation connections. Node 2 and node 4 are the rigid

beam-column connections that remain 90° before the appearance of plastic hinges near the base of columns and the ends of beams.

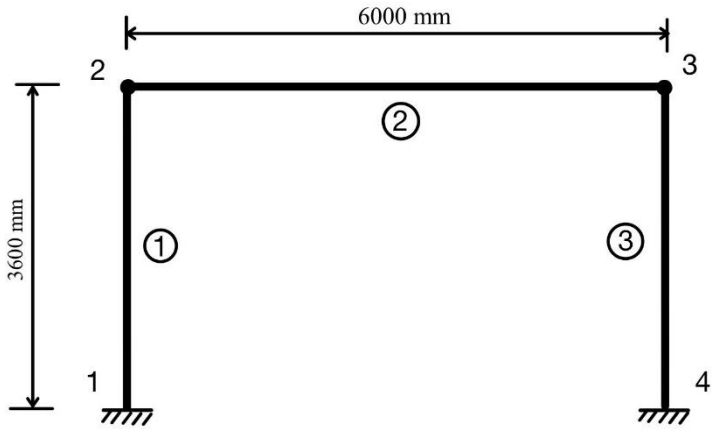

Figure 10. Idealized MF in OpenSees.

In order the consider the nonlinear behavior of members, the nonlinear Beam-Column Element is applied to the beam and columns, and there are five integration points along the length of each element with a fiber section assigned to the integration points. The steel type ASTM A36 is modeled by executing the command uniaxial material Steel 02 which is assigned to each fiber in the elements of beam and columns. The command "uniaxial material Steel 02" was introduced into OpenSees based on the well-known uniaxial constitutive nonlinear hysteretic steel material modal proposed by Menegotto and Pinto and extended by Filippou, who improve the model by adding isotropic strain hardening effect. The material Steel 02 was assumed the yield strength of 250 MPa because the conventional minimum yield strength of ASTM A36 is 36 kips in Imperial System and 250 MPa in Metric System. The elastic modulus and strain-hardening ratio were set as 200 GPa and 0.002, respectively. The other parameters $R_0 = 18$, cR1 $= 0.925$, cR2 $= 0.15$, a1 $=$ 0, a2 $= 1$, a3 $= 0$, a4 $= 1$ are defined based on the recommendation in OpenSees command manual [40].

To demonstrate the accuracy of the simulation of MF, the modal analysis and pushover analysis were performed before adding the dampers. Modal analysis is to study the dynamic properties in natural frequency, which is important for structures because if the natural frequency of the building may match the frequency of the expected earthquake, serious structural damage may be suffered due to resonance. The single-story MF was performed in ETABS and OpenSees, respectively, to compare the accuracy of the simulation of MF. As known to all, modal analysis is an eigenvalue problem, so it can be solved from the equation given by:

$$([K] - \omega^2[M])\{\varphi\} = 0 \tag{8}$$

where $[K]$ is stiffness matrix, ω is circular natural frequency, $[M]$ is mass matrix and $\{\varphi\}$ is the eigenvector or mode shape. The basic form of an eigenvalue problem given by:

$$[A - \lambda I]x = 0 \tag{9}$$

where A is a square matrix, λ is eigenvalues, I is an identity matrix, and x is an eigenvector that is corresponding to stiffness matrix, square of circular natural frequency, mass matrix, and mode shape, respectively. From Eq. (8) and Eq. (9), the relationship $\omega^2 = \lambda$ can be concluded [41]. Since the single-story MF is simulated as an SDOF system, so the eigenvector in Eq. (9) only has one entry. In this paper, λ was produced from modal analysis executed through OpenSees, as listed in Table 2., the difference of the natural periods between two software is 1.12%, so it

Table 2. Comparison of Modal Analysis

	Eigenvalues	Circular Frequency (rad/sec)	Period (sec)	Natural Frequency. (Hz)
OpenSees	286.6	16.9	0.371	2.69
ETABS	-	-	0.375	2.66

demonstrated that the modeling results in ETABS and OpenSees are very close, which means the result of modal analysis produced from OpenSees can be accepted and used in other analyses.

Pushover analysis is to determine the deformability and strength of the system. The lumped mass was gradually pushed in the horizontal direction at the beam level, causing the shear force and bending moments to rise in columns. At some point, the unrecoverable yielding of steel causes the formation of the plastic hinges appearing near the base of columns. Also, plastic hinges will appear at some later points that are close to the ends of beam. Before doing the pushover analysis, the maximum elastic deformation is calculated by hand as below, which is done by following what Malhotra et al stated in [39]. The purpose of hand calculation is to verify the accuracy of numerical modeling in OpenSees. The lateral force after the occurrence of all the plastic hinges is given by:

$$F_p = \frac{2\left(M_{pb} + M_{pc}\right)}{H} \tag{10}$$

where M_{pb} is plastic moment capacity of the beam cross-section; M_{pc} is plastic moment capacity of the column cross-section; H is equal to the height of the MF. Plastic moment capacity can be given by the following expression [42]:

$$M_p = Z_p F_y \tag{11}$$

where Z_p = section modulus; F_y = yield strength of steel. The value of $F_p = 669\ kN/mm$ can be calculated by substituting the M_{pb} and M_{pc}, listed in Table 1, into Eq. (8). The elastic stiffness, before the occurrence of plastic hinges, is given by:

$$k = m\left(\frac{2\pi}{T}\right)^2 \tag{12}$$

Substituting period T = 0.371 sec and lumped mass m = 78400 kg into Eq. (10) gives the

stiffness of the structure that is k = 22.486 kN/mm. The maximum elastic deformation D_e = 25.3 mm is produced by substituting F_p and k into the following equation:

$$D_e = \frac{F_p}{k} \tag{13}$$

In the pushover analysis, 700 kN was gradually applied to the roof level of the MF with 1mm per step, then repeat this process with 650kN. As shown in figure 10, the blue circle line and the red line, which represent the 700kN and 650kN applied respectively, are overlapped thoroughly, which means the same results were produce whatever the applied force. Point 1 denotes the maximum elastic deformation D_e and the corresponding shear force F_p generated in the columns. The D_e is around 25mm that is close to the results of the hand calculation showed above, but there is a gap of near 100 kN for F_p, since the hand calculation ignored the transition from elastic to plastic branch for simplifying the

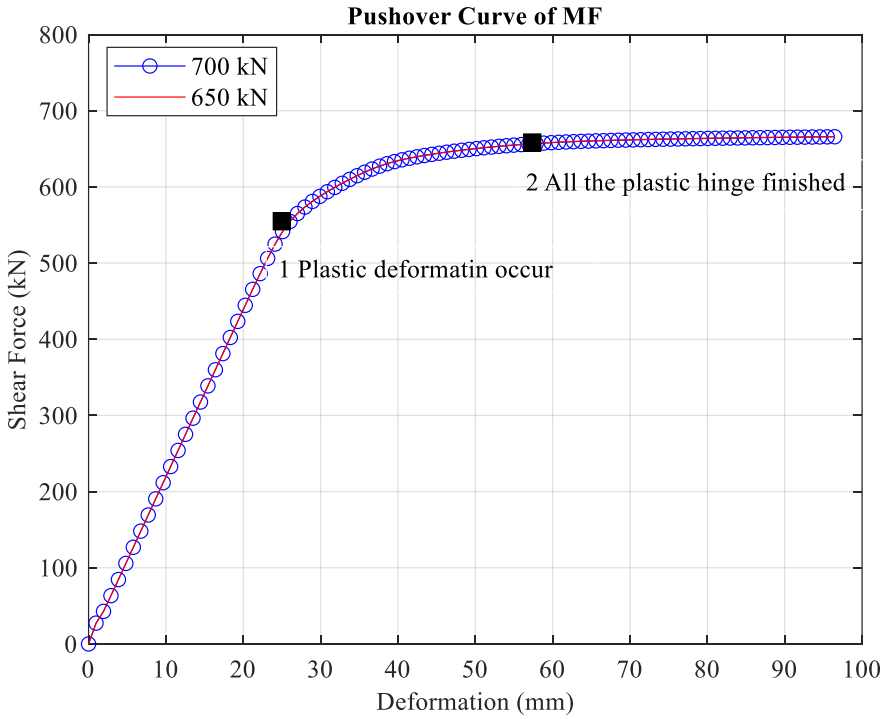

Figure 11. Pushover Curve of MF

calculation. However, the transition exists in the practical steel tensile test. Point 2 represents the ending of the stage of the elastic deformation. The project of point 2 on the y-axis is close to the result of hand calculation $F_p = 669$ kN/mm. Therefore, the simulation of the moment frame in OpenSees can be considered accurate enough for further analyses.

3.2. Modeling of MR Dampers

MR dampers based on the Bouc-Wen model (BW), the Bouc-Wen-Barber-Noori model (BWBN), as well as the conventional viscoelastic (VE) damper model, are constructed in OpenSees. Due to the dominant status of the VE damper in the study of reducing structural response, it will be clearer to learn about the performance of the MR dampers by comparing them with the VE damper model.

There are a variety of commands in the material library of OpenSees, which is still growing as more and more new material models were introduced utilizing the C++ programing language. Fortunately, although the Bouc-Wen model and BWBN model are not common in conventional FEM simulation software such as ABAQUS, ANSYS, they have been added into the material library of OpenSees. Because the constitutive relations of MR dampers are too complex to describe their behavior with only one component, mostly, they are composed of linear springs, dashpots, and special modules such as the Bouc-Wen or BWBN element.

3.2.1. Bouc-Wen Model

Wen et al introduced the Bouc-Wen model which has been applied by Spencer et al to describe the force-displacement relationship of MR damper [43], the constitutive relation of the Bouc-Wen model has been given in Eq. (6), where α is the ratio of post-yield

stiffness to elastic stiffness, k_0 is equal to elastic stiffness, c_0 is considered as viscous damping coefficient [see figure 8]. β, γ, and A are the parameters applied to evolutionary variable z that is controlling the shape of the hysteresis loop of MR-BW [26]. Based on the constitutive relation and the schematic model of MR-BW, figure 12 plots the force-velocity

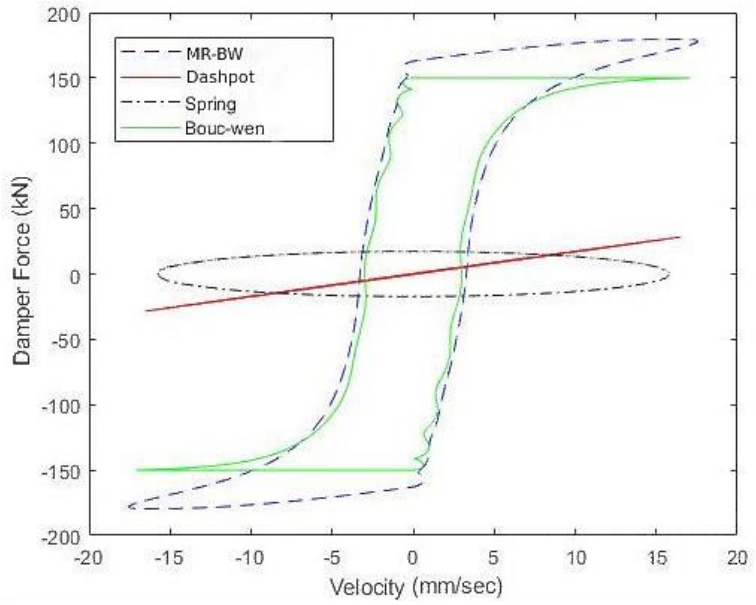

Figure 12. Phenomenological Model of MR damper: Typical Hysteretic curve of damping force versus velocity

relationship of the elastic spring, viscous dashpot, Bouc-wen element, and MR-BW to illustrate the correlation among these components. The combination of the viscous dashpot and the elastic spring leads to the tails at the end of the hysteresis loop. The skewness of the tails is close to the slope of the red line represented by the dashpot.

There are four material commands were used for the modeling of MR-BW: The command “uniaxialMaterial Elastic” is able to describe the behavior of elastic spring for tension and compression; “uniaxialaxialMaterail ViscousDamper” were employed to depict the behavior of the dashpot if the spring stiffness was set as zero; The material

"UniaxialMaterial BoucWen", which is an extension of the original Bouc-Wen Model but include stiffness and strength degradation [44], was applied to represent the Bouc-Wen module as shown in figure 8; the command "uniaxialMaterial Parallel" can construct a parallel material object made up of the first three components [40]. There are many parameters involved in the Bouc-wen model, however, some parameters were not defined such as the Ao, δ_A related to tangent stiffness, and δ_ν, δ_η are about the material degradation, because they don't fit the Bouc-wen module as Spencer et al stated in [26]. All the parameters are summarized in Table 3. Figures 13(a) and 13(b) show the simulated hysteretic response of MR-BW under 0.5Hz sinusoidal excitation.

Table 3. MR-BW parameters

	α $(kN.mm^{-1})$	k_0 (kN. mm^{-1})	c_0 $(kN.s.mm^{-1})$	γ (mm^{-2})	β (mm^{-2})	n	Ao	δ_A	δ_ν	δ_η
Bouc-Wen	14	0.175	0.5	0.2	0.8	2	1.0	0	0	0

α is initial elastic stiffness
k_0 is the stiffness of elastic spring in tension and compression
c_0 is the damping coefficient of the dashpot in figure 7(a)
γ, β, Ao, n are the hysteretic parameters and $\delta_A, \delta_\nu, \delta_\eta$ are related to tangent stiffness and material degradation

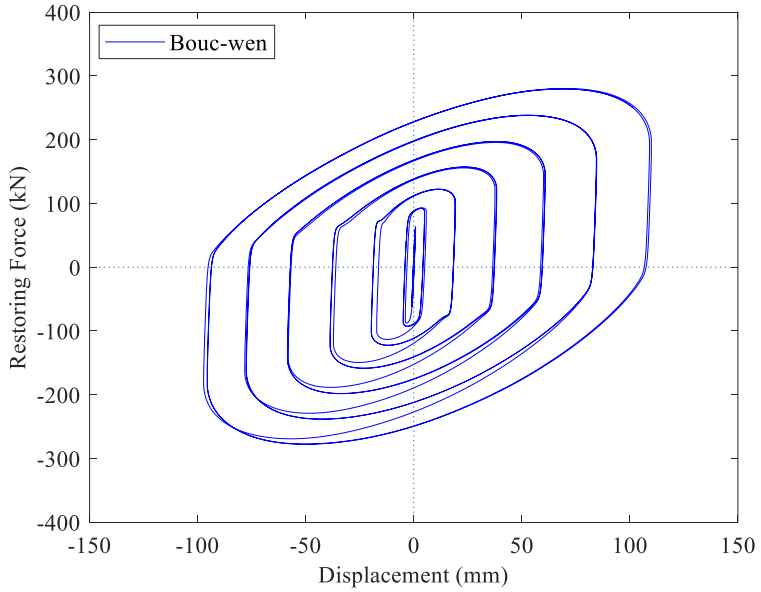

(a)

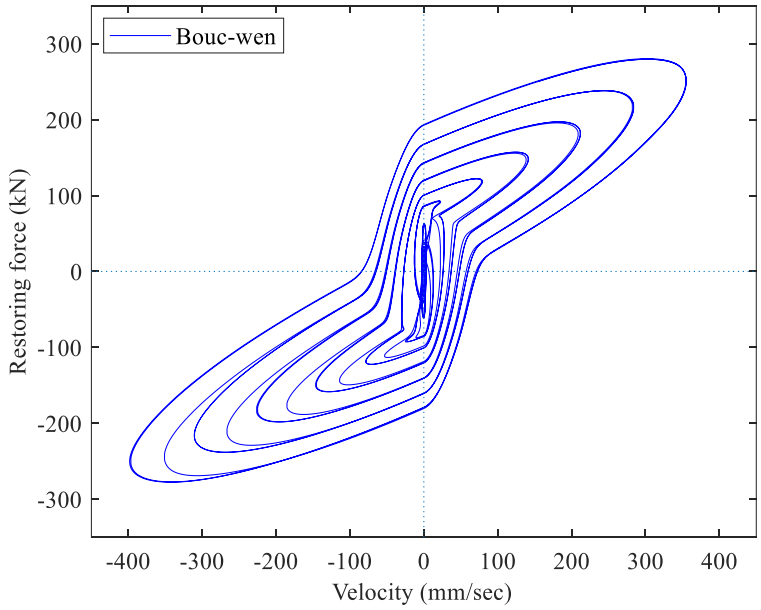

(b)

Figure 13. Hysteresis curve of MR-BW

3.2.2. BWBN Model

Baber and Noori proposed smoothly varying deteriorating hysteretic models based on the Bouc-Wen model, incorporating time history-dependent postyield restoring forces and general pinching behavior [44]. Peng et al stated that the typical Bouc-Wen model sometimes cannot handle the irregularity of hysteresis sufficiently, therefore, a new MR damper model with the BWBN model adopted was proposed [45]. The main visible difference between the MR-BWBN and MR-BW is the pinching in the force-displacement relationship of MR-BWBN that exhibits higher irregularity than the MR-BW, as shown in figures 15 (a). The damper force of MR-BWBN is expressed in a set of differential equations that are given by:

$$F = \alpha F_i u(t) + (1-\alpha) F_i z + c_0 \dot{u}(t) \tag{14}$$

Eq. (14) demonstrates that the nonlinear restoring force of MR-BWBN is made up of elastic and hysteretic components, as well as a dashpot to describe the bending that formed at the

peak of each damping cycle, as illustrated in figure 14. The parameter α is the ratio of post-yield stiffness to the initial elastic stiffness, F_i is the initial elastic stiffness. The non-degrading pinching hysteretic response depends on the hysteretic displacement z which is expressed by the following equations as:

$$\dot{z} = \frac{\dot{u}(t)h(z)\{A - [\gamma + \beta\,\mathrm{sgn}(\mathrm{u(t)}\dot{z})]|z|^n\}}{\eta} \tag{15}$$

where pinching inducing function $h(z)$ is given by:

$$h(z) = 1.0 - \zeta_1 e^{\left(-(z\cdot sgn(\dot{\delta}) - qz_u)^2/\zeta_2^2\right)} \tag{16}$$

$$z_u = \left[\frac{1}{v(\beta+\gamma)}\right]^{\frac{1}{n}} \tag{17}$$

$$\zeta_1 = \zeta_{1o}\left[1 - e^{(-p\varepsilon)}\right] \tag{18}$$

$$\zeta_2 = \left(\psi_0 + \delta_\psi \varepsilon\right)(\lambda + \zeta_1) \tag{19}$$

$$\dot{\varepsilon} = (1-\alpha)F_i z\dot{u}(\mathrm{t}) \tag{20}$$

The parameters A, γ, β, and n are the same as in the Bouc-Wen model that decides the shape of the hysteresis loop. The parameter ν and η are responsible for controlling the strength and stiffness degradation. ζ_1 ranging from 0 to 1 decides the degree of pinching, ζ_2 is about how the pinching region spread. z_u and q are the model parameters. z_u is the ultimate value of z in Eq. (14). ε decides the magnitude of ζ_1 and ζ_2 and represents the

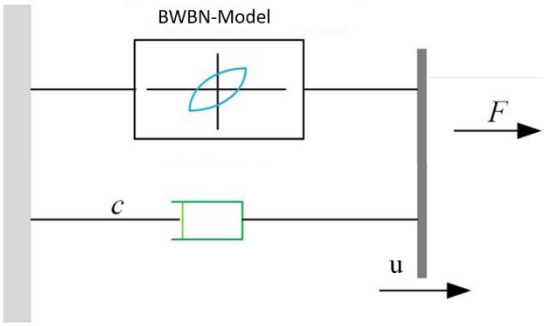

Figure 14. Mechanical model of MR-BWBN

dissipation of hysteretic energy. In addition, parameter p controls the rate of the initial drop in the slop, ζ_{1o} controls the total slip, ψ_0 is one of the parameters related to the amount of pinching, δ_ψ is specific for the rate of pinching spread, λ decides the rate of change of ζ_1 and ζ_2 [45]. Hossain et al have developed BWBN model, which was applied to MR-BWBN mentioned in this paper, in the form of "uniaxialMaterial BWBN" in OpenSees [46]. The parameters $\alpha = 0.00524$, $\gamma = 0.5$ mm^{-1}, $\beta = 0.5$ mm^{-1}, A = 1, n = 1.213 are estimated constants, all the other parameters are listed in Table 4.

Table 4. BWBN parameters

	F_i (kN.mm^{-1})	q	λ	p	ψ_0	δ_ψ	ζ_{1o}
BWBN	14.175	0.3	0.0002	0.012	0.22	0.0001	0.95

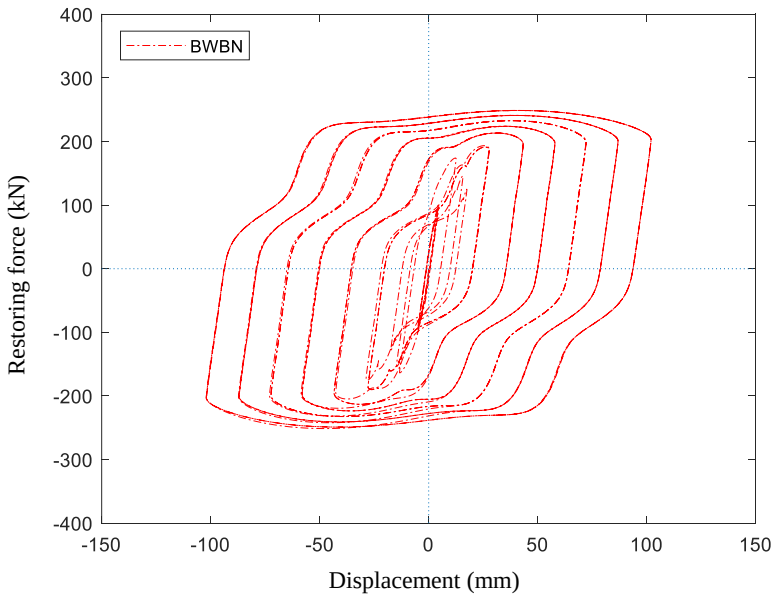

(a)

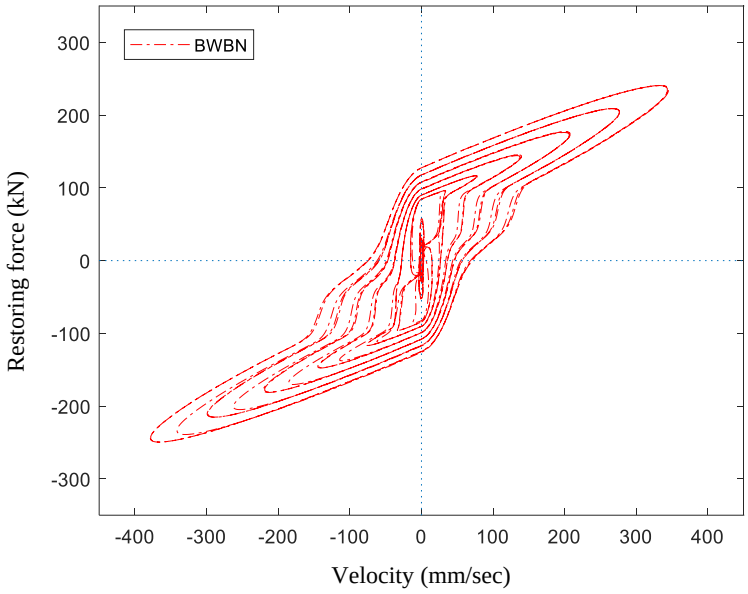

(b)

Figure 15. Hysteretic curve of MR-BWBN

3.2.1. Viscoelastic Dampers (VE)

As mentioned in the section of MR-BW, the Bouc-Wen model is in parallel with an elastic spring plus a dashpot. The combination of elastic spring in parallel with a pure viscous damper is the prototype of viscoelastic material that is also called Kelvin-Voigt. It has broad applications from passive damping to aircraft tire construction [47]. Due to the popularity of the Kelvin-Voigt model in the modeling of viscoelastic damper, comparing the performance of MR-BW and MR-BWBN with VE will be more concise and explicit, also, the work done by Bouc-Wen module in MR-BW may be more apparent. The constitutive relationship of VE is given by:

$$F = k_0 u(t) + c_0 \dot{u}(t) \tag{21}$$

The stiffness elastic spring $k_0 = 14.175$ kN.mm^{-1}, and the damping coefficient $c_0 = 0.5$ kN.s.mm^{-1} are estimated constants. For VE damper, figure 16 (a) and figure 16 (b) give the hysteretic response of force-displacement relationship and force-velocity relationship under 0.5 Hz sinusoidal excitation, respectively.

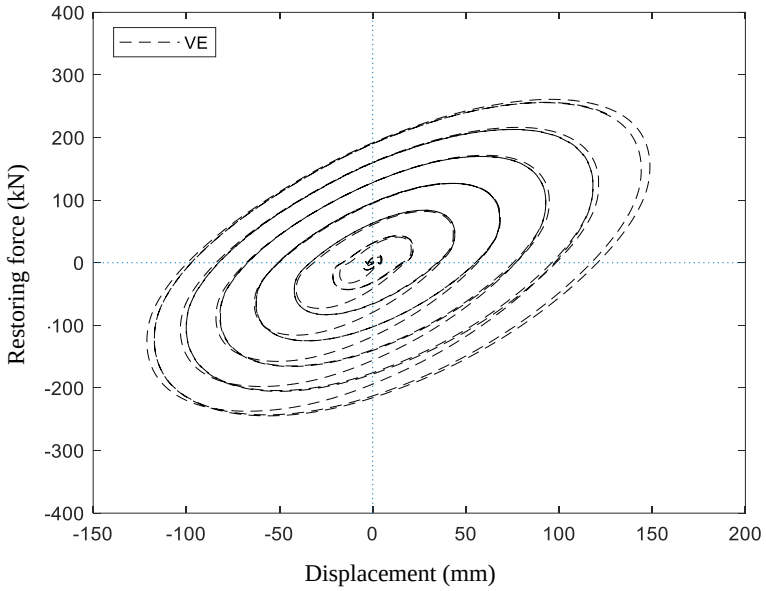

(a)

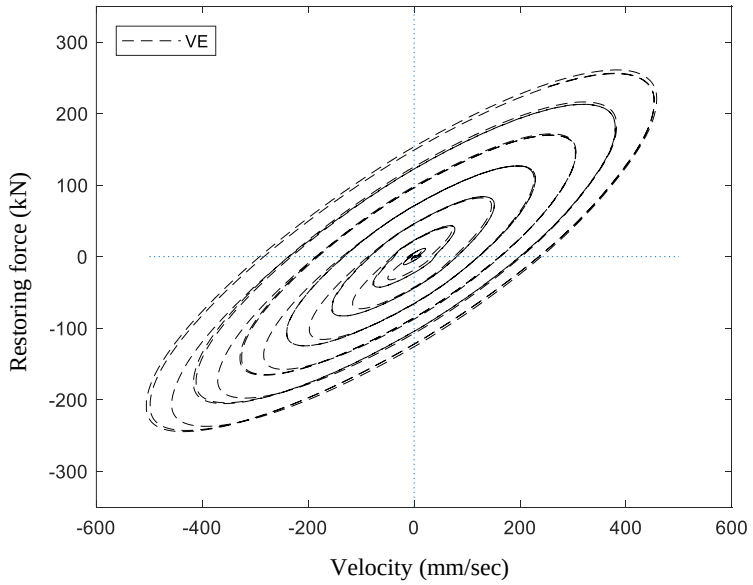

(b)

Figure 16. Hysteretic curve of VE

3.3. Ground Motions Considered for Analyses.

As mentioned in the introduction chapter, more than 150 buildings suffered serious damage during the Northridge earthquake. Therefore, one of the seismic records of the Northridge earthquake, as recommended in FEMA P695, is selected to evaluate the performance of the MR dampers applied to a Single-story MF during a horizontal ground shaking. The recording site of the selected seismic record is on Mulholland Drive in Beverly Hills whose closest distance to the fault is 17.4 km [48]. As the distance of the recording site to the fault is more than 15 km, it is considered a far-filed record as suggested in UBC-97 [49]. The peak ground acceleration (PGA) of the selected ground motion for simulation are scaled to 0.2g, 0.4g, and 0.588g, corresponding to a basis -level earthquake with a 10% probability of exceedance in 50 years, a rare earthquake associated with a 2% probability of exceedance in one year, and a 0.01% probability of exceedance in 50 years [50] [see figure 17].

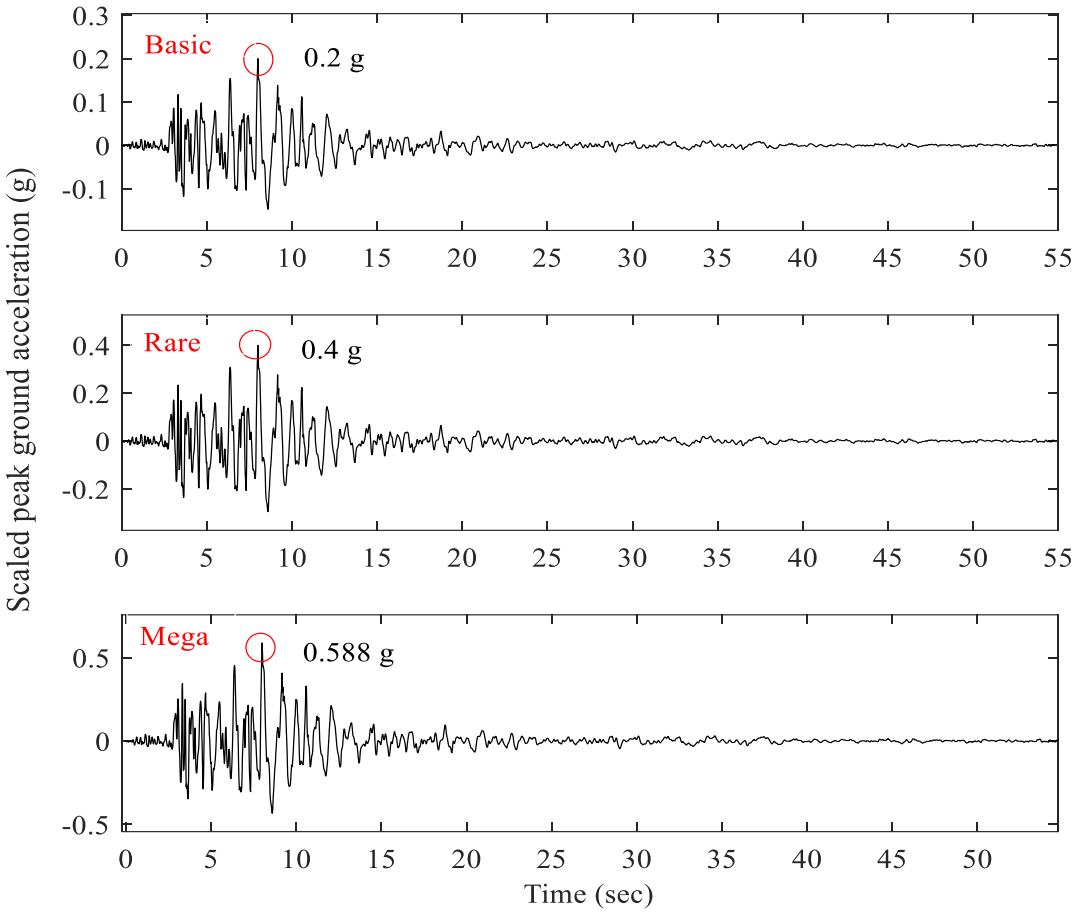

Figure 17. Scaled ground acceleration of the Northridge Earthquake (N-S)

Chapter 4. Analyses

4.1. Introduction

Mass (weight), lateral strength, deformability, and damping are the key characteristic of a structure. Mass(weight) is the physical property of a structure. Lateral strength is the structure's ability to resist the horizontal load. Deformability is its ability to deform laterally. Structure's ability to quickly dissipate vibration energy is damping. For structures with specific damping, more deformation means less strength to withstand ground vibrations. While for specific deformability, a more damped structure needs a smaller strength to withstand ground shaking.

The analysis for structural response to ground motions can be static or dynamic. Static analyses do not require the solution of the equations of (EOM) while dynamic analysis does require it. Response spectra are used in static analysis for various values of damping while dynamic analyses use ground motion histories. There are four basic types of analyses: (1) linear-static, (2) linear-dynamic, (3) nonlinear-static, and (4) nonlinear-

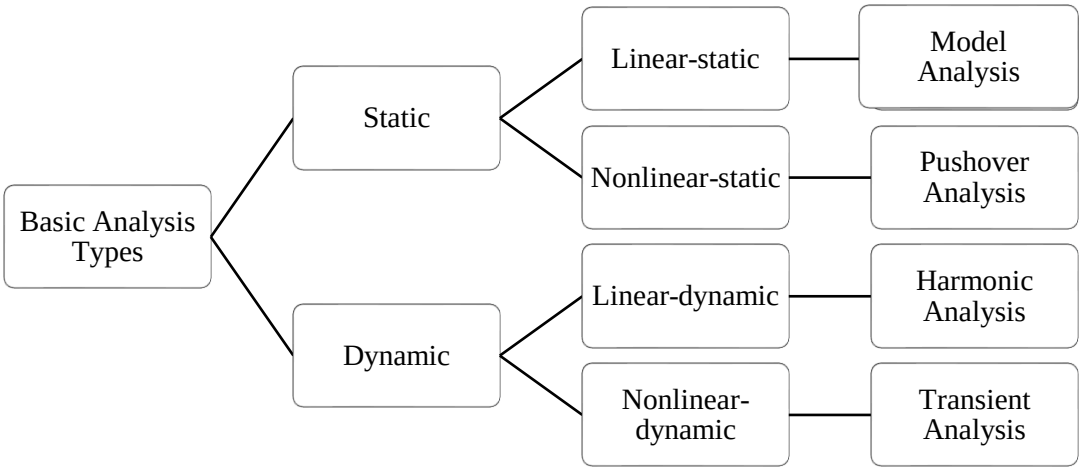

Figure 18. Basic Analysis Types

dynamic, as shown in figure 18 [39]. Modal analysis, harmonic analysis, and transient analysis are presented in the following sections, pushover analysis is not talked about herein for the static response of the MR dampers are the not the focus in the application of seismic resistance.

4.2. Modal Analysis

Modal analysis is to determine the natural frequencies of structures that is one of the aspects of dynamic properties. Mode analysis is a sort of linear-static analysis. It is essential in structural engineering, because once a building's natural frequency matches the frequency of expected earthquakes in the area where the building is located, it may experience severe structural damage due to resonance that results in large oscillation. Except for the earthquake, wind, mechanical vibration, and human activities such as footstep pulse also may excite a structure's natural modes.

In practice, modal analyses are significant for buildings that have more than one story. To decide the full response to the given loading, mode superposition is utilized in the conventional FEM software [51]. For the multi-story structure, the effective modal mass and modal participation factor can decide the significance of a vibration mode when processing modal analysis. The modal participation factor is a measure of the contribution of a given mode for the structural response subjected to ground excitation. The modal participation factor for the i^{th} mode is given by:

$$\Gamma_i = \frac{\boldsymbol{\phi}_i^T \boldsymbol{M}\boldsymbol{r}}{\hat{m}_{ii}} \tag{22}$$

where $\boldsymbol{\phi}_i$ = i^{th} mode shape, $\boldsymbol{M}$ = the mass matrix of the whole system, $\boldsymbol{r}$ is the influence factor that represents the displacement of the masses resulting from a static unit ground displacement

[52]. For the one-bay multiple-story structure, the participation factor for the first modes is much larger than the other modes, and the effective modal mass of the first mode can reach 90% of the total mass of the system, which means the one-bay multi-story structures can be idealized as an SDOF system. The motion of equation of SDOF system including damping is given by the following expression:

$$m\ddot{u} + c\dot{u} + ku = P_0 \sin(\omega t) \tag{23}$$

The damping ratio ζ can be given by:

$$\zeta = \frac{\mathrm{c}}{2\mathrm{m}\omega_\mathrm{n}} = \frac{\mathrm{c}}{2\sqrt{\mathrm{km}}} \tag{24}$$

and the natural frequency of damped vibration ω_n can be expressed as:

$$\omega_D = \sqrt{\frac{k}{m} - \frac{c^2}{4m^2}} \tag{25}$$

However, the paremter “c” is damping coefficient including damping owned by the system itself as well as the additional damping from the damper system. It is so small that can be ignored comparing with structural stiffness “k”, so the $\omega_D \approx \omega = \sqrt{\frac{k}{m}}$. With the same stiffness, damping coefficient, and mass, whichever damper model was used, the MF has the same natural frequency. It is widely known that structural stiffness and damping decide elastic deformation limit. To compare the performance of different damper models, the contrast experiment method was utilized for the analyses process where spring stiffness and damping keep the identical for all the test cases. However, the addition of the dampers inevitably contributed to the stiffness and the damping of structures and then increased the natural frequency of the whole SDOF system. The natural frequency of the SDOF system may vary from the different damper stiffness, the higher stiffness the additional dampers have, the higher natural frequency the whole structure

will achieve, as shown in figure 19.

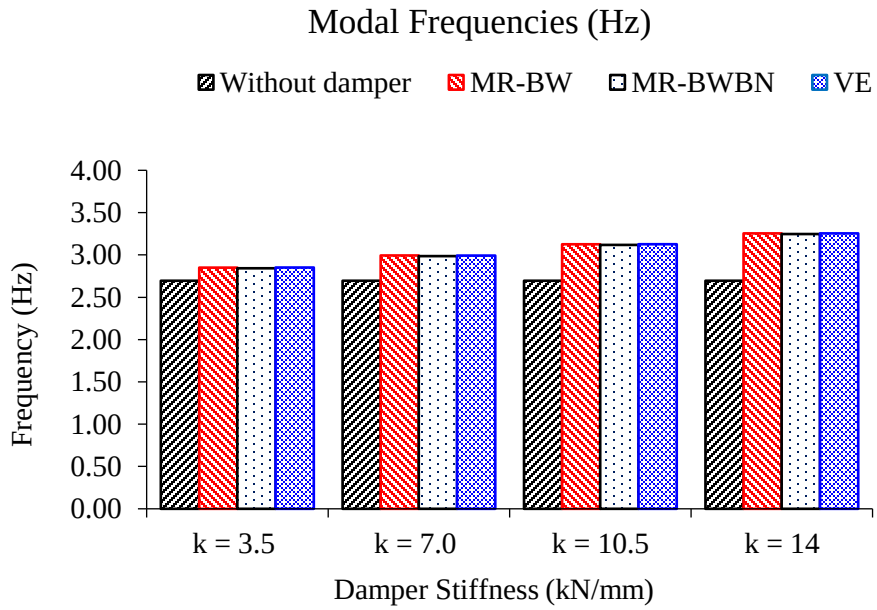

Figure 19. Modal Frequencies

Table 5 lists modal frequencies of the systems applied dampers whose stiffness are 3.5 kN.mm^{-1}, 7.0 kN.mm^{-1}, 10.5 kN.mm^{-1}, and 14 kN.mm^{-1}, respectively. It should be noted that the modes are basically an inherently a linear concept as it is a method to reduce the model size and reduce computational work. It is well known that the lower natural frequency the building has, the more possible the structure resonance may occur under the irregular external excitation. In addition, the added mass of the dampers may decrease the natural frequency, but it is too small to be considered comparing with the mass of the whole structural system. The natural frequency of the common MF without damper system is 2.69 Hz, by comparison, the increase of the structural natural frequency can be up to 20.8% when the stiffness of the additional damper reaches 14 kN/mm, which is a large amount of change that is high enough to be taken advantage of to control the natural frequency for structural seismic resistance design.

Table 5. Natural Frequency of SDOF with Damper

	λ	ω (rad.sec^{-1})	T (sec)	f (Hz)
k_D = 0 kN.mm^{-1} (without damper)	2.87E+02	16.9	0.371	2.69
k_D = 3.5 kN.mm^{-1}	3.21E+02	17.9	0.350	2.85
k_D = 7.0 kN.mm^{-1}	3.53E+02	18.8	0.335	2.99
k_D = 10.5 kN.mm^{-1}	3.84E+02	19.6	0.320	3.12
k_D = 14.0 kN.mm^{-1}	4.18E+02	20.4	0.307	3.25

4.3. Harmonic Analysis

Harmonic analysis is a method to determine the steady-state response of a structure subjected to a sinusoidal (harmonic) loading to a given frequency. The process includes the calculation of the structural response to a series harmonic loading with various exciting frequencies and plotting a graph of the structural response versus corresponding frequency. The peak harmonic response resulted from large oscillation due to the structural resonance when the forcing frequency is infinitely close to the natural frequencies of structures. The structural harmonic response will be amplified if the frequency of the external excitation matches the natural frequency and mitigated of the forcing frequency away from the natural frequency of the structure. The differential equation, which includes viscous damping, governing the response of SDOF system to harmonic load is given by:

$$m\ddot{u} + c\dot{u} + ku = p_o sin\omega t \tag{26}$$

The solution of steady-state response Eq. (26) is expressed by:

$$u(t) = Csin\omega t + Dcos\omega t \tag{27}$$

$$C = \frac{p_o}{k} \frac{1 - \left(\frac{\omega}{\omega_n}\right)^2}{\left[1 - \left(\frac{\omega}{\omega_n}\right)^2\right]^2 + \left[2\zeta\left(\frac{\omega}{\omega_n}\right)\right]^2} \tag{28}$$

$$D = \frac{p_o}{k} \frac{-2\zeta\left(\frac{\omega}{\omega_n}\right)}{\left[1 - \left(\frac{\omega}{\omega_n}\right)^2\right]^2 + \left[2\zeta\left(\frac{\omega}{\omega_n}\right)\right]^2} \tag{29}$$

where p_o is the amplitude of the force, ω is the exciting frequency. The damping ratio ζ is 0.05 for all the test cases as it is owned by the system itself. The Eq. (27) is not the complete solution of the governing differential equation, because the free response, which also was called transient response is negligible because it eventually decays exponentially with frequency ratio (ω/ω_n) and damping ratio ζ, and only the steady-state response remains that is also the focus in the following discussion [41]. Harmonic analysis is not included in the command manual of the OpenSees, so the analysis was done by imposing a series of sinusoidal wave that the frequency varied from 0.375 Hz to 9.75 Hz in increments of 0.25 Hz to obtain the peak values of the lateral displacement at the roof level of the structure. The acceleration amplitude is 4.8 m/sec^2. The plot of the response quantity is in the function of (ω/ω_n), as shown in figure 20.

Figure 20 shows the peak response occurred at the point $\omega/\omega_n = 1$, which coincides with the statement about the structural resonance in the beginning. The results of the harmonic response of the three damper models are close to each other at each frequency, so the plot of the harmonic response of the three damper models are almost overlapped. In addition, Eq. (28) and Eq. (29) indicate that the structural peak response relies on the structural stiffness k, structural natural frequency, and damping ratio. and the applied force is linear dependent, so the higher exciting force will cause severer damage to

buildings when the exciting frequency is close to the structure's natural frequency, which can be utilized to predict the structural peak response when subjected to harmonic loads with various of amplitude such as wind load. However, in the reality, the exciting force is usually applied to the structure when it is under the dynamic motion, like modal analysis, harmonic analysis is also a strongly linear analysis that the nonlinearity of the elements is ignored in FEM software. Therefore, considering the high nonlinearity of MR dampers, the transient analysis has to be performed to explore the dynamic response of the SDOF system under the seismic loadings.

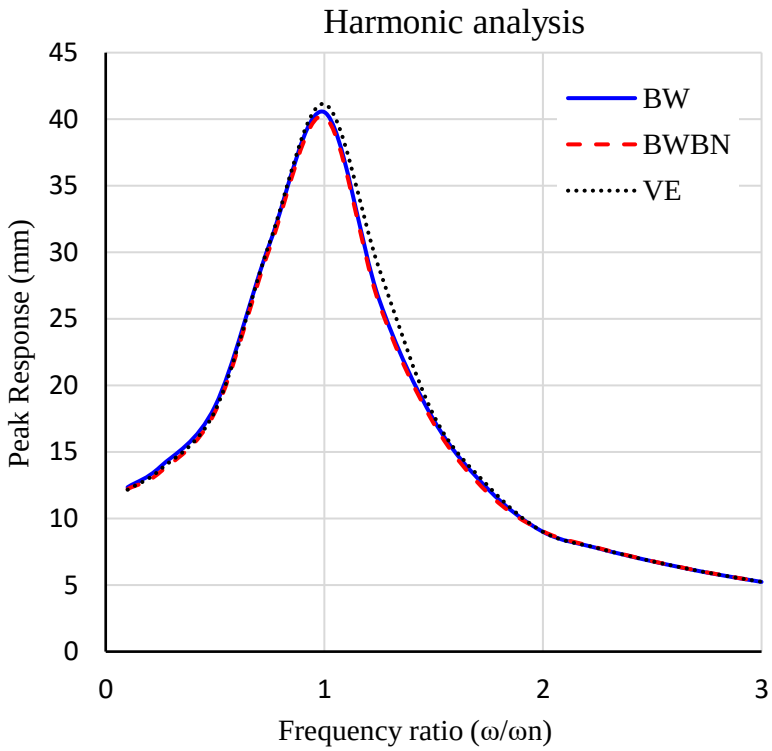

Figure 20. Harmonic frequency response curve

4.4. Transient Analysis

As discussed in previous sections, the work done by the nonlinearity of the MR damper models was hidden in linear analyses, in order to investigate the effect of MR dampers in seismic resistance, transient analysis has to be performed. Transient analysis sometimes is also called time-history analysis, just as its name implied, the analysis is caried out with the force varying with respect to time. It is routinely performed via direct time integration procedure. Besides, transient analysis is well known as a more accurate method to determine how well these MR dampers will perform during a seismic event, because the nonlinear damping and inertia effect, which is not included in static analyses but important in dynamic analyses, are considered [53].

As mentioned in the chapter 1, energy conservation rule can be utilized to explain how the dampers work on a building. For example, during an earthquake event, a building in the seismic region will receive the input energy from the ground motions due to earthquake activities, they will be dissipated by the structural vibration, instantaneous elastic deformation, damping, and hysteresis, which are corresponding to kinetic energy, strain energy, damping energy and hysteretic energy in Eq. (2), respectively. Thus, the energy dissipation devices can improve the performance of structures via increasing the damping and hysteresis ability to reduce the energy dissipated by the other two parts, vibration and deformation of the components. Therefore, except for story drift ratio, the energy dissipation can be an aspect to measure the effect of MR dampers in seismic resistance as well.

4.4.1. Cyclic Loading

Four test cases went through transient analyses, including MF with Bouc-Wen model, MF with BWBN model, MF with VE damper, and a common MF. Before inputting the actual earthquake data as the ground motion, SAC prescribed cyclic load [see figure 21] was applied in the horizontal direction on the roof level in which the lumped mass was located [54]. The strain and stress were generated at the fiber near the bottom of columns that have been fixed to the ground, as the shear force and moment are the maxima at that point where the column start to deform.

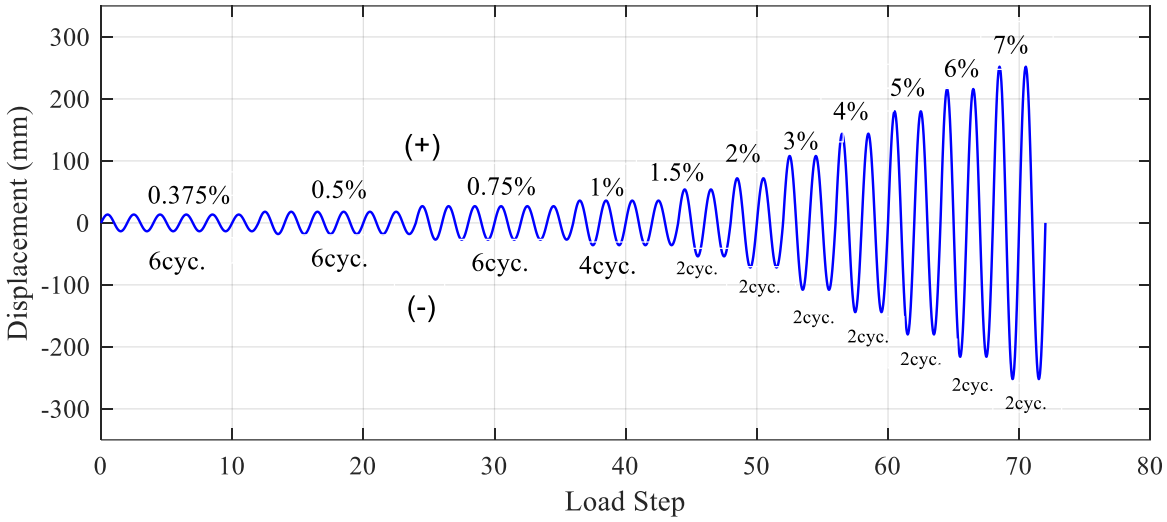

Figure 21. Prescribed SAC Loading [61]

The strain energy mentioned here results from the instantaneous elastic deformation, and unrecoverable plastic deformation, which is part of hysteresis. Figure 22 illustrated the structure of strain energy in the form of stress-strain hysteretic curve. The plastic strain energy is represented by the area enclosed by the hysteretic curve, while the elastic strain energy is the area between the horizontal coordinate axis as well as the elastic parts of the curve [55]. Although in the field of structural engineering, some important

components can be protected through the method that designing the plastic hinge zones at the end of the beams intentionally to help dissipate energy, the plastic deformation is not desired because the irreversible deformation is a big challenge for the sustainability. Hence, an effective energy dissipation device should have the capability to reduce the tendency of plastic deformation.

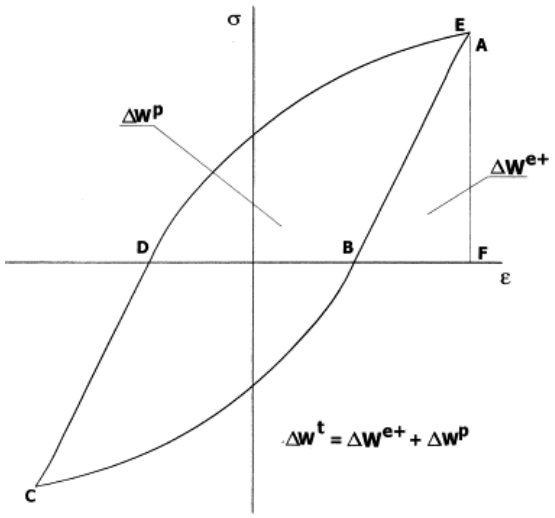

Figure 22. Elastic and Plastic energy [59]

The stress-strain relationship of the plastic deformation has been applied to all the test cases, as exhibited in figure 23. As mentioned in the previous sections, the stiffness of all the test cases have been defined as the same values, which is demonstrated by the identical slope of the elastic parts in stress-strain curve. In addition, the area enclosed by the hysteretic curve in figure 23 (b) corresponding to the BWBN mode is the smallest among the others, and figure 23 (a) related to the Bouc-Wen model came second. The cumulative plastic strain energy of MR-BW, MR-BWBN, VE, and MF are produced by integrating the area enclosed in the stress-strain hysteresis loop exhibited in figure 23, and the results were shown in figure 24. It shows that the cumulative plastic strain energy of MR-BW, MR-BWBN, VE, and MF are 2904 J, 2695 J, 3809 J, and 4642 J, respectively. Figure

25 shows the energy change tendency with respect to time for the MF-BW, in the first 45 seconds, the exciting displacement is very small, so all the energy change are small as well, to examine the energy dissipation during this period, one point around t = 25 sec was amplified. It shows the strain energy at that point is zero without any energy accumulation, which demonstrates the structures have not entered the phase of plastic deformation. As the applied displacement gradually goes up, the structural deformation exceeded the elastic deformation limit, then the irreversible deformation occurred.

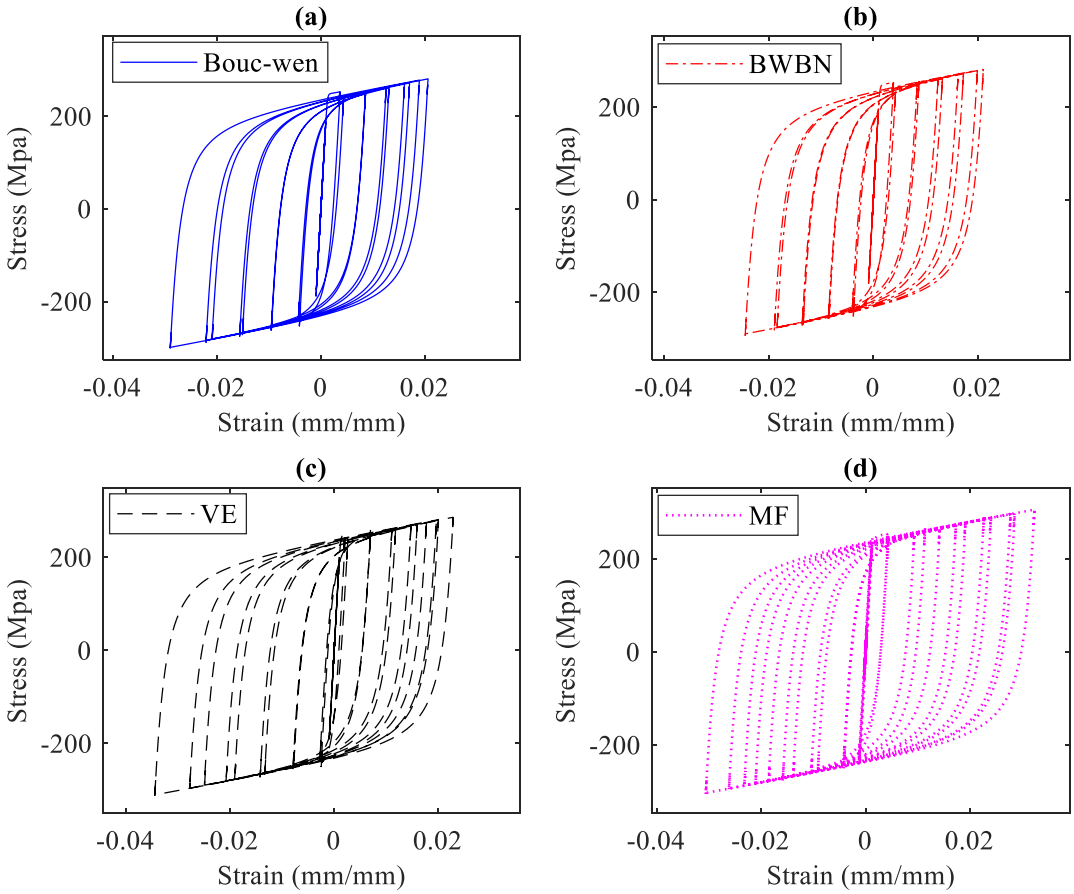

Figure 23. Stress-strain history curve:(a) Bouc-wen model; (b) BWBN model; (c) Viscoelastic damper; (d) without damper

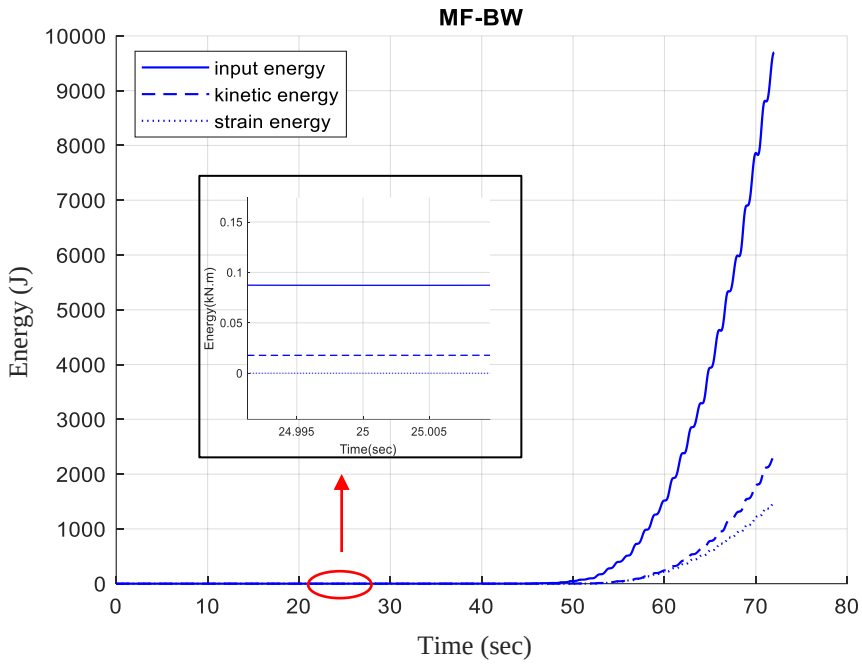

Figure 25. Energy change history

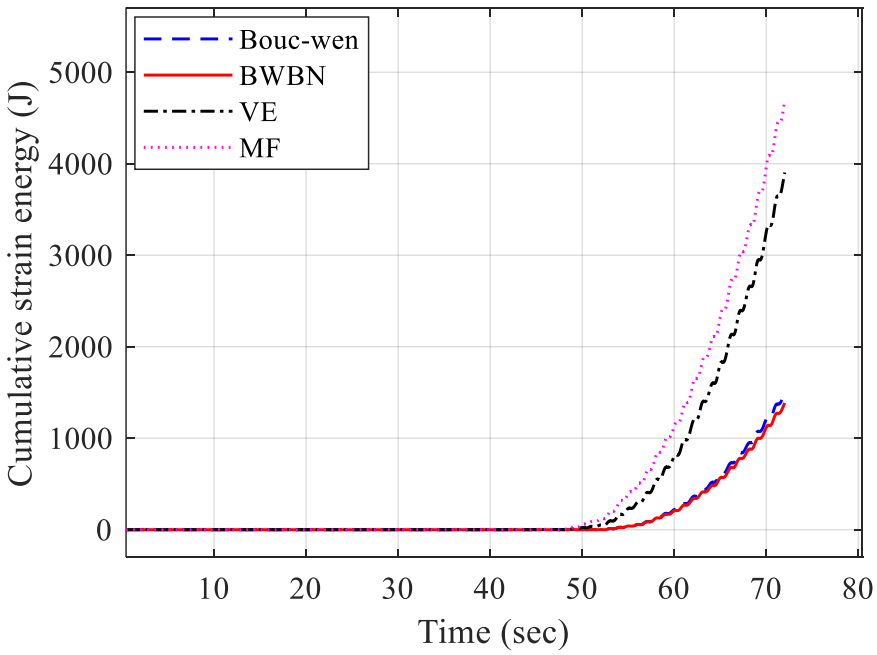

Figure 24. Cumulative strain energy

Without any changes to the modeling, the transient analysis was repeated while the applying displacement on the beam level was replaced by cyclic ground acceleration. Due to the reason that the huge amount of data cannot illustrate the difference clearly in only one figure, some segments extracted from the full time-history can be seen in figure 26 that the MR damper group had less lateral displacement than the other two models throughout the full time-history on the roof level. Mostly, the peak values of the lateral displacement of MR-BW and MR-BWBN are almost overlapped. However, during the period from the $t = 14$ sec to $t = 20$ sec, the amplitude of the lateral displacement of MR-BWBN is slightly higher than MR-BWN, which is 24.14 mm while the MR-BW is 20.22 mm at $t = 18.864$ sec. Nevertheless, as the amplitude of the ground acceleration increase, this phenomenon reversed in the compression near the end of time, the amplitude of the lateral displacement of MR-BWBN came up to 119.74mm as the MR-BW reach 128.1mm. These test results told the fact that the MR-BWBN might be less sensitive to the violent ground motions than MR-BW, and this conjecture was confirmed by the subsequent transient analysis with an actual earthquake ground acceleration applied.

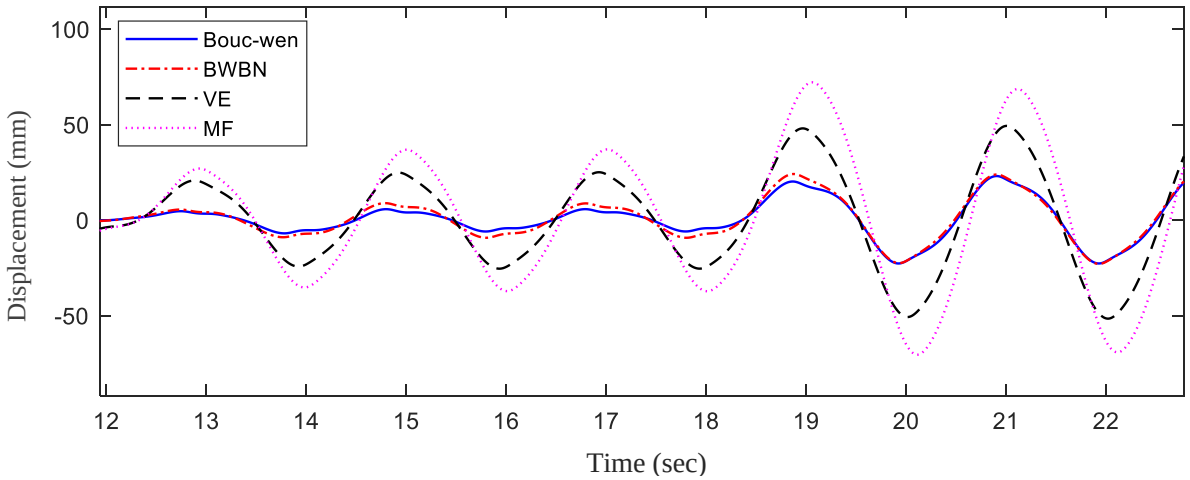

(a)

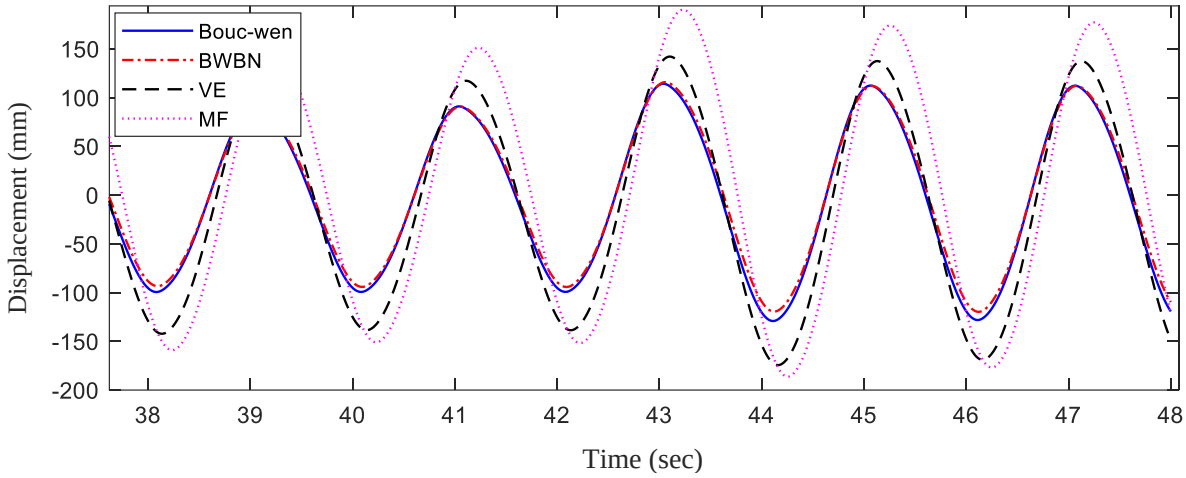

(b)

Figure 26. Lateral displacement of roof level

4.4.2. Seismic Loading

Again, the transient analysis was performed under the same conditions to examine the seismic response with the dampers applied, except for the ground motion replaced by the Northridge earthquake 1994 recorded on the Mulholland Drive in Beverly Hills, in addition to the absence of the common MF on account of the unsatisfactory performance proved in the previous analyses. The peak ground acceleration (PGA) of the selected ground motions had been scaled to 0.2g, 0.4g, and 0.588g corresponding to a basic-level earthquake with a 10% probability of exceedance in 50 years, a rare earthquake associated with a 2% probability of exceedance in one year, and a 0.01% probability of exceedance in 50 years [50].

Figure 27 shows the maximum drift ratios of MR-BW, MR-BWBN, and VE are 0.011, 0.013, 0.015 for the basic level, 0.031,0.029, 0.036 for the rare level, 0.053,0.049,0.059 for the mega level, respectively. The time history of lateral displacement plotted in figure 28 demonstrated that the performance of MR-BWBN during the basis-level earthquake seems not ideal in reducing the structural response in tension comparing with MR-BW and VE, but

still the best in compression. As the PGA goes up, the gap of the peak value among the three types of damper models reduced in tension while increased in compression.

In addition, the earthquake hysteretic response was simulated using MR-BWBN to compare the behaviors of MR-BW and VE. Figure 29 shows the pinching phenomenon using MR-BWBN in hysteretic response of force-displacement were gradually mitigated under the large earthquake, but the ability of deformation resistance was not reduced but improved as the ground acceleration increase.

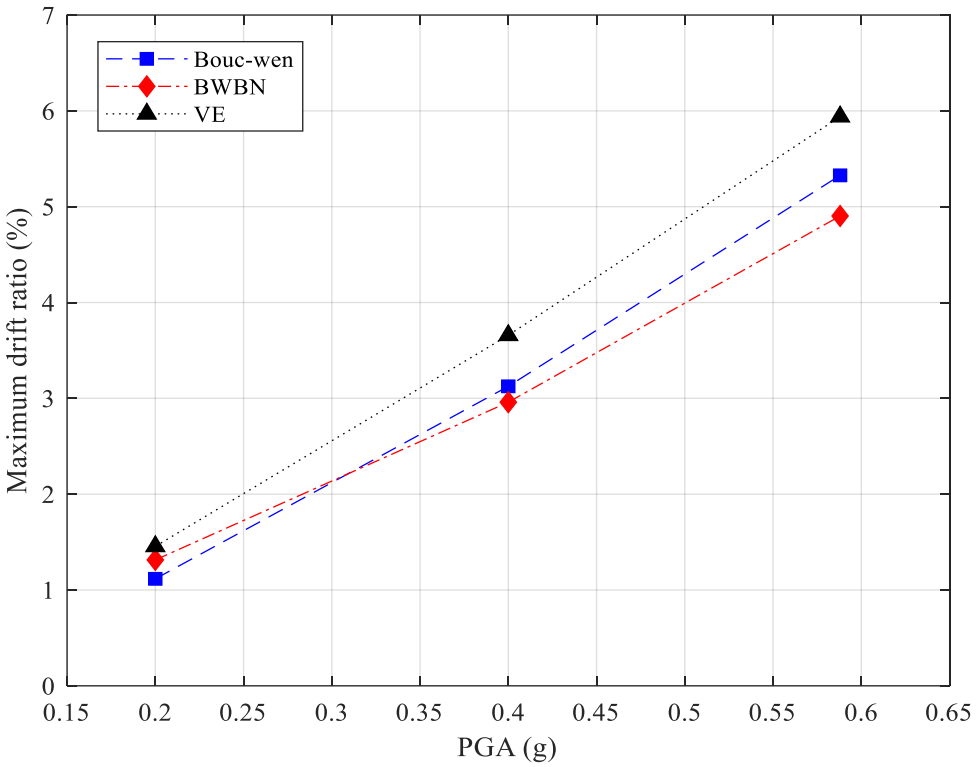

Figure 27. Maximum drift ratio

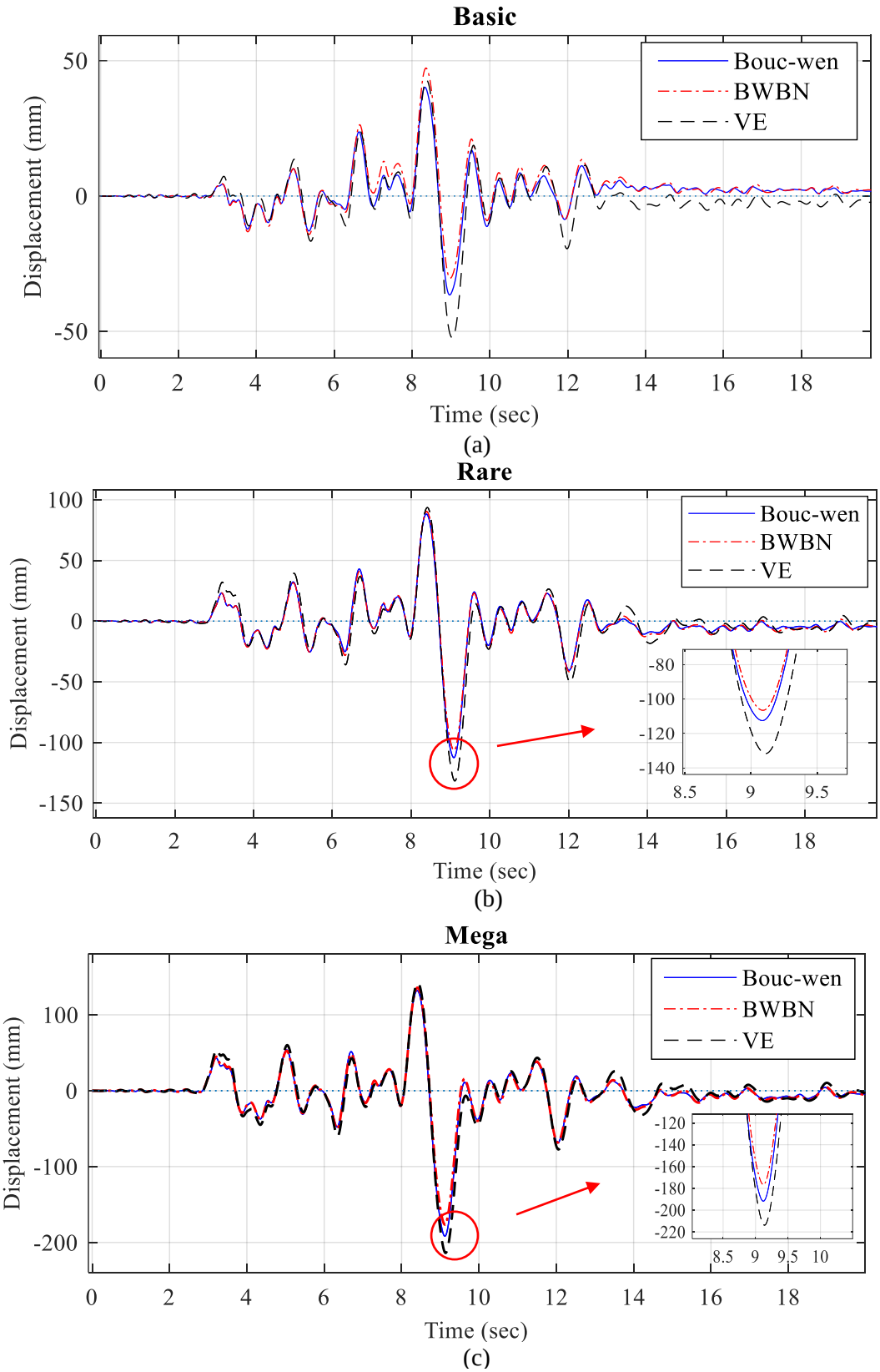

Figure 28. Lateral Displacement of Roof Level Under the Earthquake of: (a) Basic; (b) Rare; (c)Mega

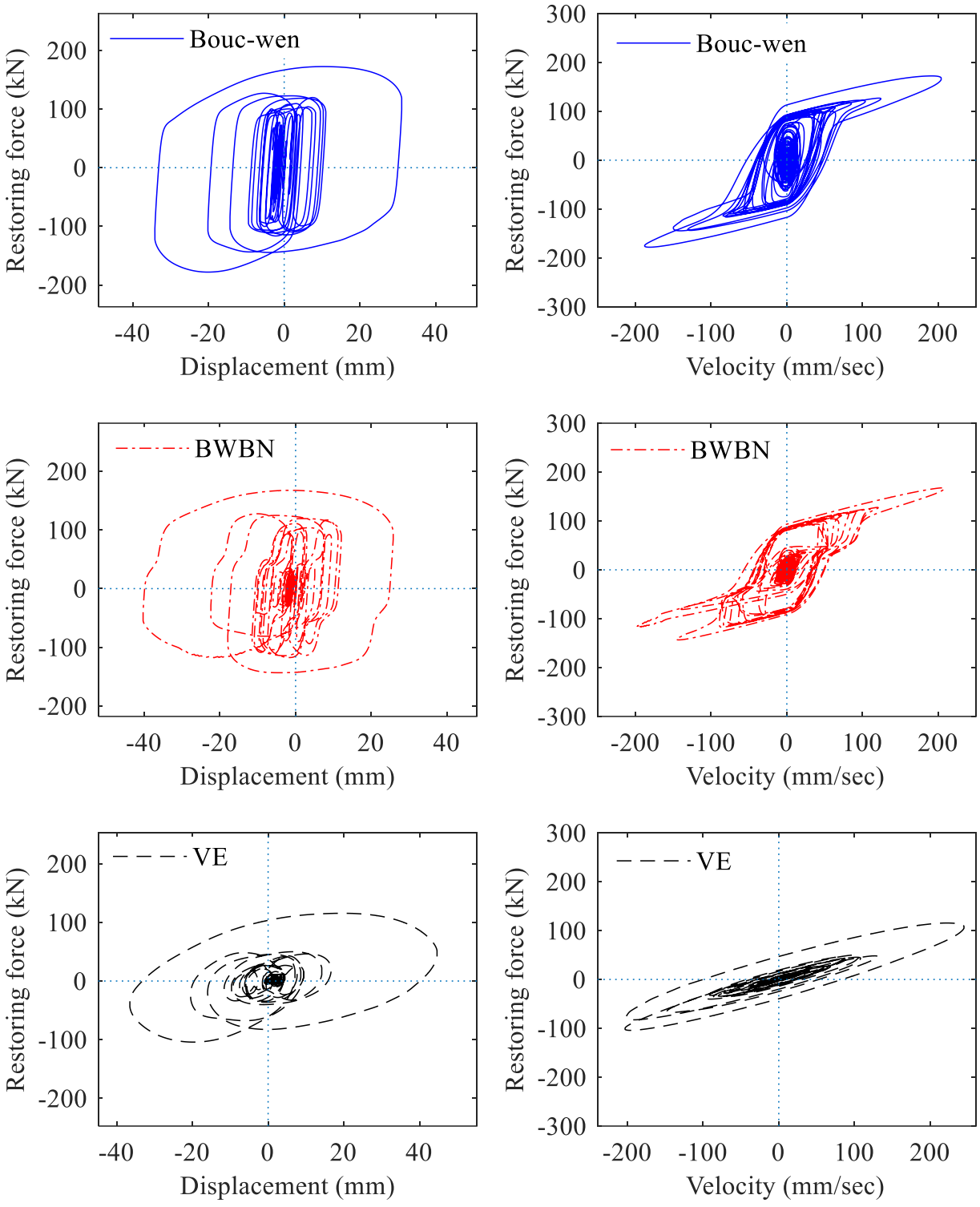
Bouc-wen
Restoring force (kN)
Displacement (mm)
Velocity (mm/sec)
BWBN
VE

(a)

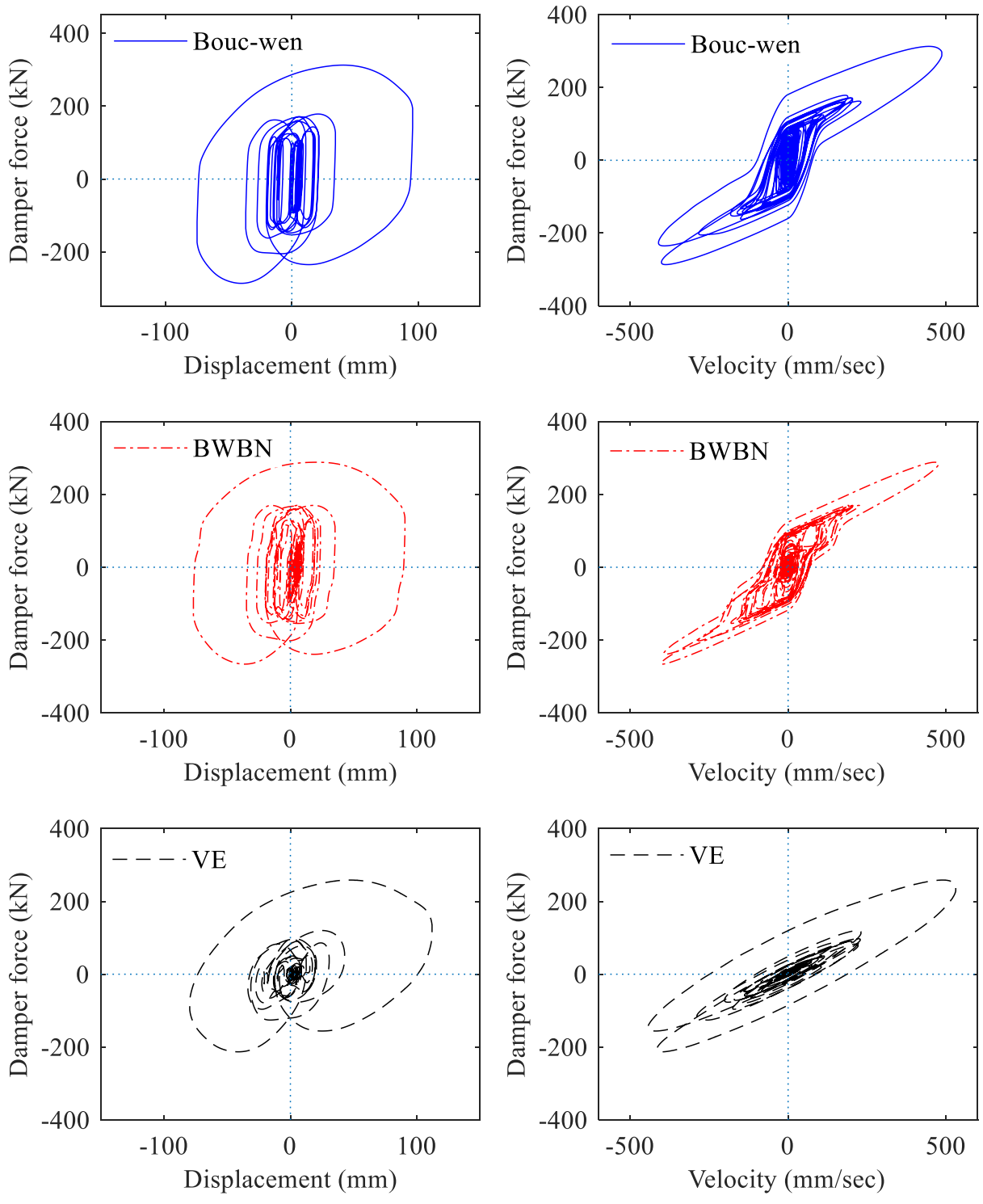
Bouc-wen
Damper force (kN)
Displacement (mm)
Velocity (mm/sec)
BWBN
VE
400
200
0
-200
-400
-100
100
-500
500

(b)

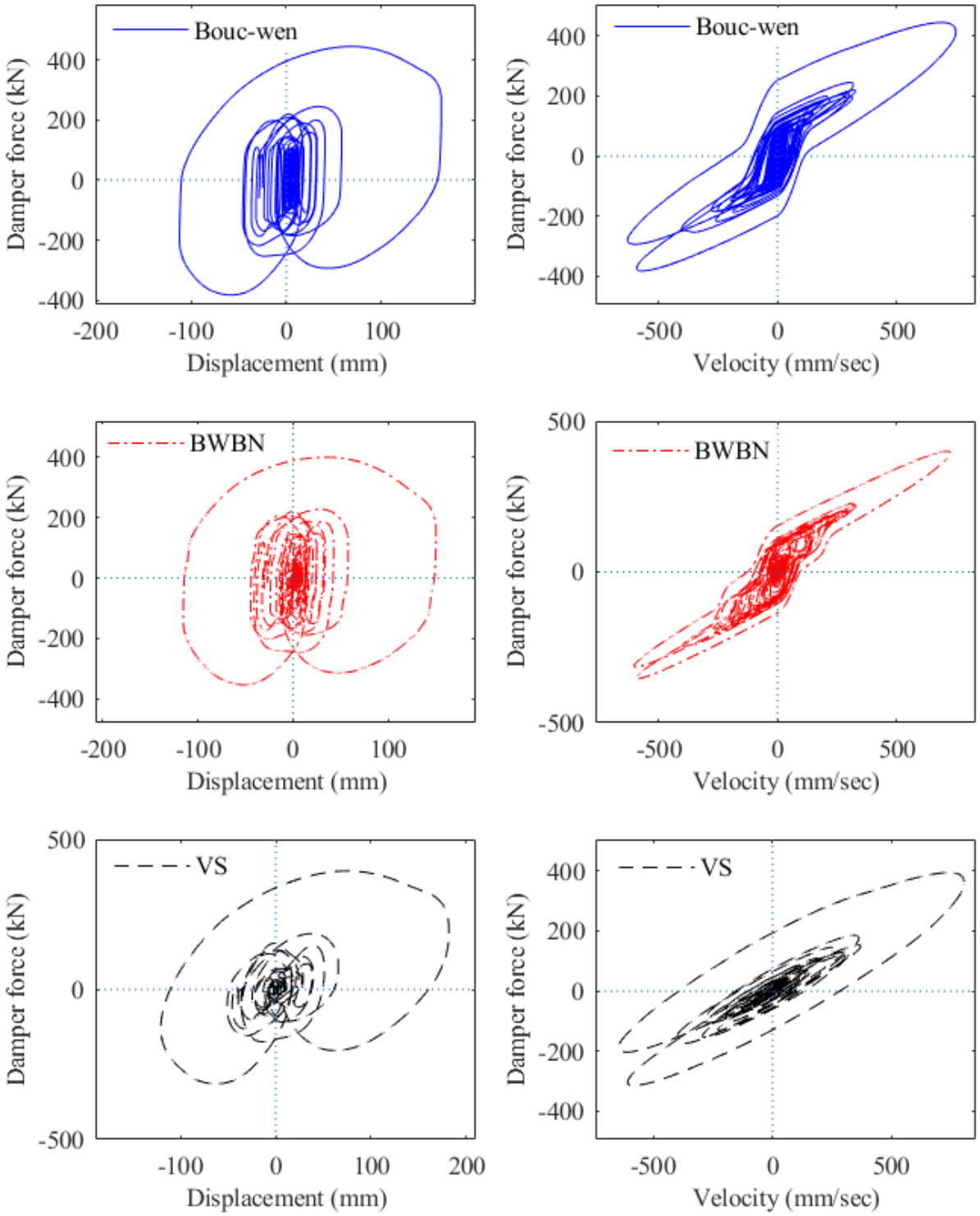

(c)

Figure 29. Hysteretic curve of MR damper and VE under the earthquake: (a) Basic; (b) Rare; (c) Mega

Other than the comparison of the lateral displacement, cumulative energy dissipation is another reference to compare how well the dampers work on the structures. Anil K. Chopra gave the formulas in his book about how to calculate the input energy, kinetic energy, as well as energy dissipated by viscous damping [41]. The input energy during the earthquake is given by:

$$E_I(t) = -\int_0^u m\,\ddot{u}_g(t)du \tag{30}$$

where $\ddot{u}_g$ is the ground acceleration, u is the velocity of the structures subjected to ground motion. The kinetic energy is related to the mass associated with its motion relative to the ground:

$$E_K(t) = \int_0^u m\,\ddot{u}(t)du = \frac{m\dot{u}^2}{2} \tag{31}$$

The damping energy is defined as follows:

$$E_D(t) = \int_0^u c\,\dot{u}(t)du \tag{32}$$

The calculation of strain energy has been explained in the previous section. According to Eq. (2), the energy dissipated by the dampers is equal to:

$$E_H = E_I - E_k - E_s - E_D \tag{33}$$

The results of the simulation were shown in figure 30, under the basic level, the cumulative energy dissipation for MR-BW, MR-BWBN, and VE are 28.6 kJ, 27.1 kJ, and 16.1 kJ, respectively; and the cumulative energy dissipation under the rare level are 135.5 kJ, 144.2 kJ, and 85.8kJ, respectively; the cumulative energy dissipation under the mega level is 147.2 kJ, 158.4 kJ, respectively. The cumulative energy dissipated by MR-BWBN is less than MR-BW by 5.9% if subjected to the basis level earthquake while higher than MR-BW by 6.42% under the

rare level earthquake, 7.6% the mega level earthquake. Besides the comparison among the dampers under the same earthquake excitation, the increase rate of the cumulative energy dissipation of the same damper under the different seismic load was also recorded, from the basic-level to rare, the increase rate of cumulative energy dissipated by MR-BW, MR-BWBN, VE is 373.7 %, 432.1%, and 432.9%, respectively; from the rare to mega, the increase rate is 8.63%, 9.84%, and 1.86%, respectively [see figure 31].

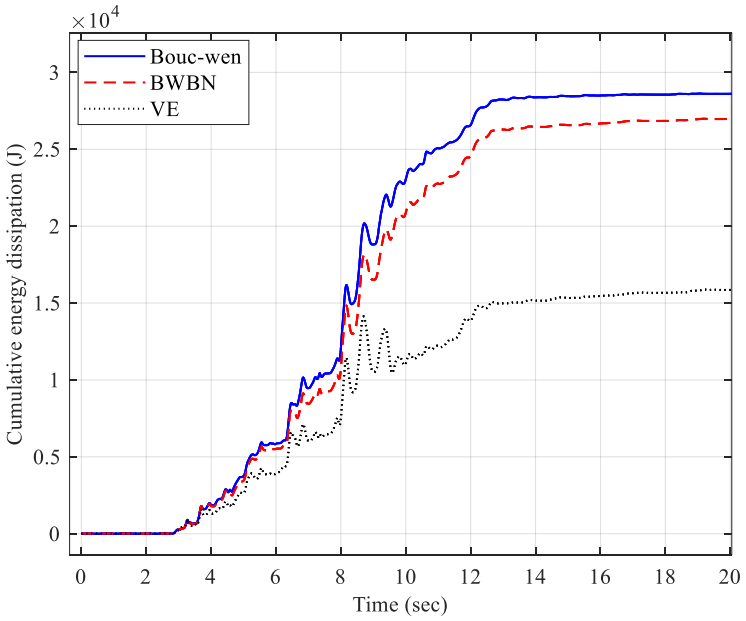

(a)

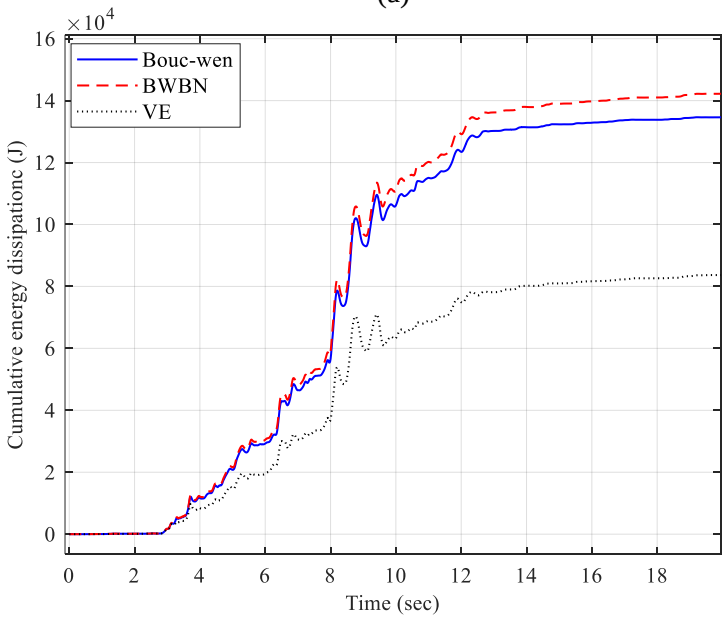

(b)

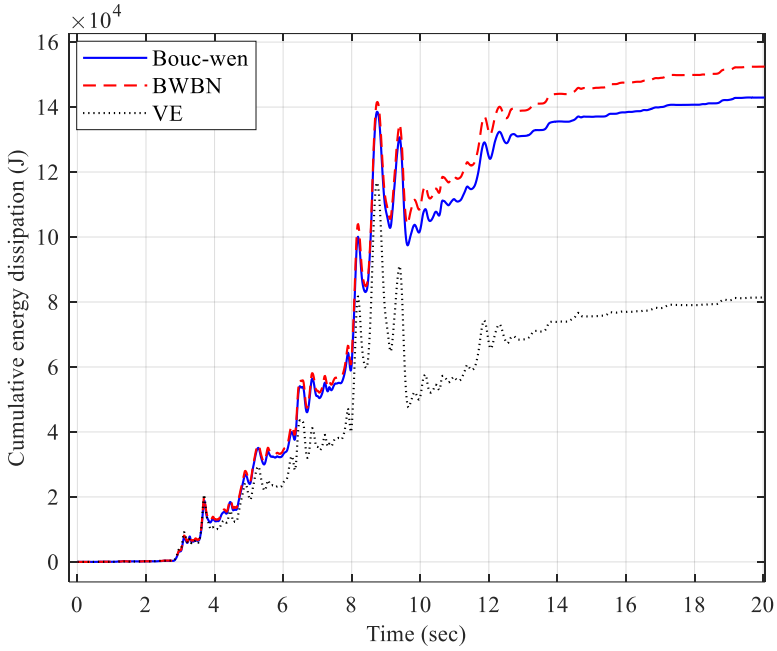

(c)

Figure 30. Cumulative Energy Dissipation: (a) Basis; (b) Rare; (c) Mega.

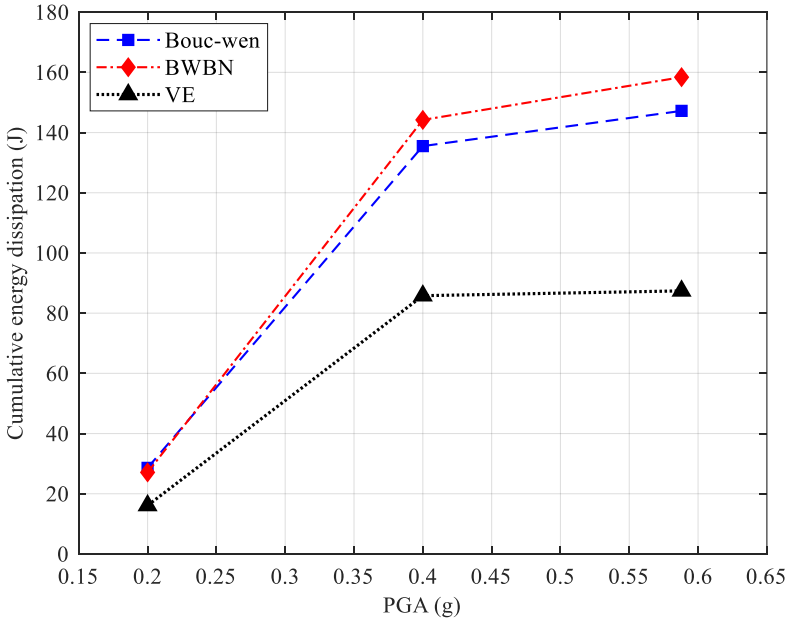

Figure 31. Peak value of cumulative energy dissipation

Chapter 5. Parametric Study

The performance of the modeling is associated with the parameters defined in the hysteretic models of the MR damper. As mentioned in chapter 1, the properties of the MR material vary from the intensity of the magnetic field controlled by electricity, thus the parameters of the MR damper models change accordingly. About MR-BW, the facts demonstrated in Spencer's work include the increase of restoring force was observed readily as the input current went up, the shape of the hysteresis loop became larger as well. The characteristic parameters α, γ, β, and n, which are responsible for describing the shape of the hysteretic curve of MR-BW, also have to be adjusted [56]. Because the BWBN model was proposed based on the Bouc-Wen model, the phenomenon of MR-BW subjected to different input current also applied to MR-BWBN to some extent. Unlike the MR-BW, the hysteretic displacement z of MR-BWBN has a pinching inducing function $h(z)$ included, as defined in Eq. (16). The parameters, k_e, c_0, and ξ_{10} in $h(z)$ control the elastic stiffness, damping, and total slip related to the pinching in the hysteresis loop of MR-BWBN, respectively. Except for α, γ, β, and n, k_e, c_0, and ξ_{10} in $h(z)$ are the parameters also influenced by the input current. As the current goes up, the value of ξ_{10}, k_e, c_0 are increased by the enhancement of the external magnetic field, which is stimulated by the electricity [44]. Because the influence of the parameters in MR-BWBN on structural response was rarely reported, the parametric study in this chapter mainly focuses on k_e, c_0, and ξ_{10}. The seismic loading of Northridge 1994 utilized in transient analysis was applied to parameter study.

5.1. Initial Elastic Stiffness

The initial elastic stiffness decides the range of restoring force that has been specified in Eq. (15). As the input current increase, the enhancement of the magnetic field causes the ferromagnetic particles more tightly packed together, which leads to higher elastic stiffness. The plot of force-displacement relationship of MR-BWBN model, under the ground acceleration of a 0.5-Hz sine wave with an amplitude of 100 mm, is shown in figure 33. The initial elastic stiffness k_e were defined as 3.5 kN.mm^{-1}, 7.0 kN.mm^{-1}, 10.5 kN.mm^{-1}, and 14 kN.mm^{-1}, respectively. Due to the complexity of the constitutive relation of BWBN model, it is hard to find the correlation between the activation force and the spring stiffness. However, increasing the initial stiffness k_e leads to a fuller hysteresis loop and larger enclosed area, which means more energy was dissipated. Higher energy dissipation resulted in a smaller lateral displacement on the roof level, as shown in figure 28(b), which is desired for the researchers of seismic dampers.

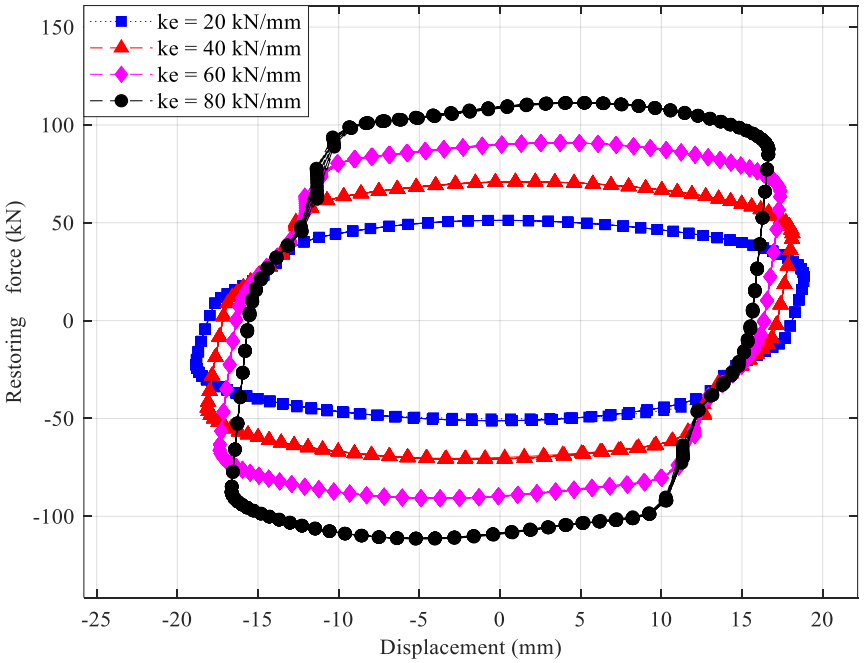

Figure 32. Hysteretic response of different elastic stiffness

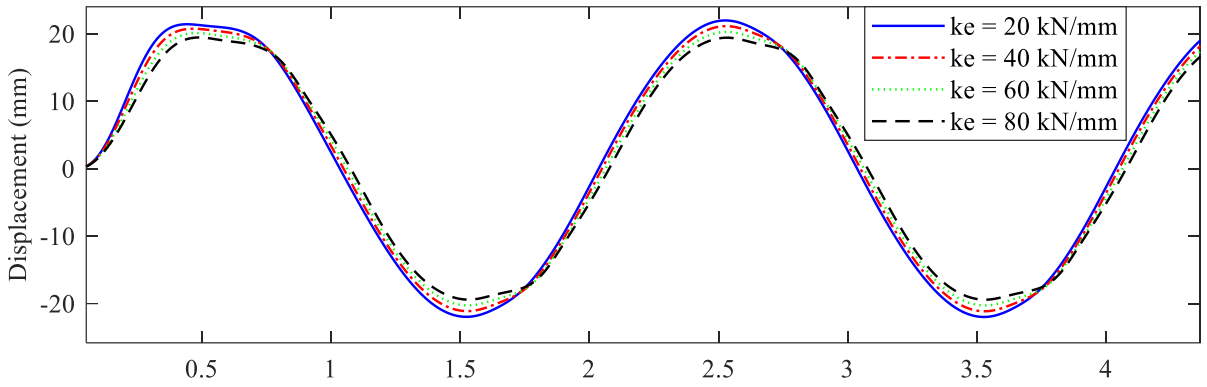

Figure 33. Lateral displacement on roof level

5.2. Damping Coefficient

Damping has the effect of reducing or preventing oscillation through the processes that dissipated the energy stored in the oscillation. Besides the inherent damping owned by the structures, the applied damper system is also one of the resources of damping. Nevertheless, the damping coefficient c_0, was exhibited as a dashpot element in the mechanical model of BWBN, is not only for energy dissipation, but to describe the behavior of MR fluid damper more accurately [45]. A harmonic loading was applied to BWBN model that is the same as mentioned in the last section. Five difference damping coefficients, $c_0 =$ 0.1 kN.sec.mm^{-1}, $c_0 = 0.2$ kN.sec.mm^{-1}, $c_0 = 0.3$ kN.sec.mm^{-1}, $c_0 = 0.4$ kN.sec.mm^{-1}, and $c_0 =$ 0.5 kN.sec.mm^{-1}, were performed, respectively. As shown in figure 34, the bending that occurred at the peak of each damping is more sudden when the damping coefficient is smaller, meanwhile, the area enclosed in the hysteretic curve is also reduced. To further explore the performance of BWBN model in energy dissipation with various damping coefficients, the seismic loading of Northridge 1994 was applied. As shown in figure 35, the energy dissipated by the viscous damping was amplified as the damping coefficient increase.

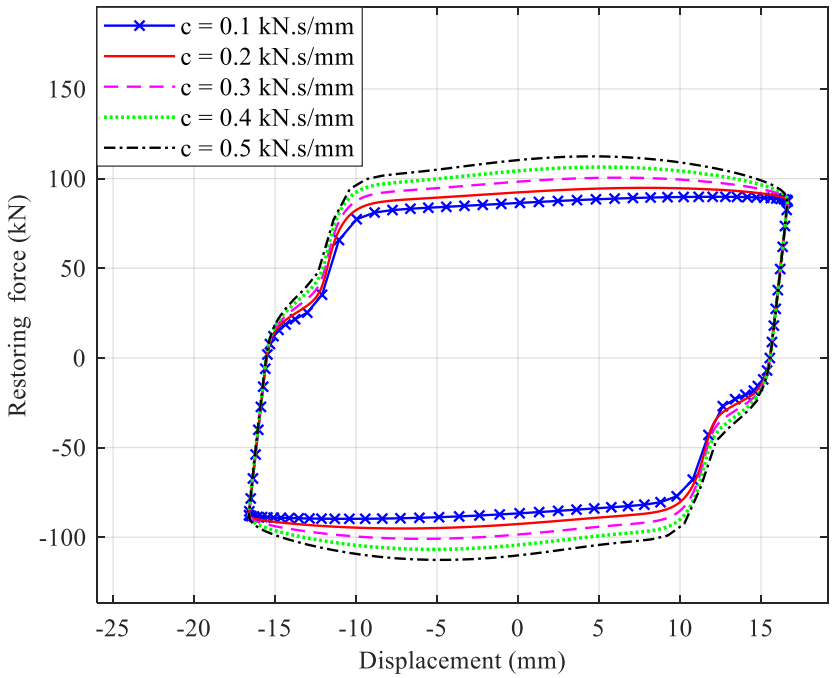

Figure 35. Hysteretic response of different damping coefficient

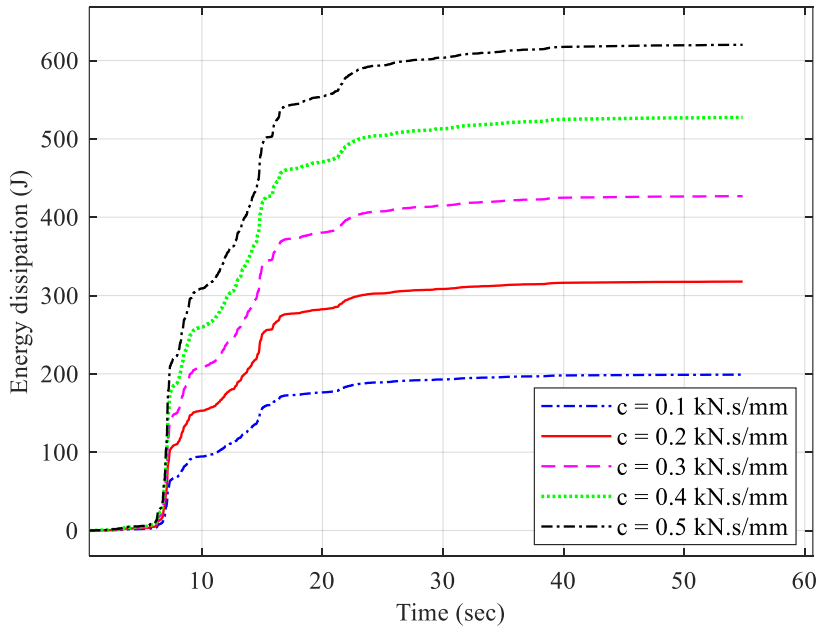

Figure 34. Comparison of damping energy

5.3. Total Slip

The obvious distinction between the parameter ξ_{10} with the first two is that ξ_{10} is just a parameter serving for the numerical simulation of BWBN model, it has not been found any correlated physical meaning. The increasing current leads to an alternation of the shape of the hysteresis loop for BWBN model, although the change is very small, the ξ_{10} has to be adjusted to fit the behavior of practical MR damper more accurately. ξ_{10} is the measure of total slip that a larger value of ξ_{10} cause a more severe pinching [45]. Figure 36 shows when ξ_{10} is equal to 0.99, the shape of hysteretic curve lost pinching at the bottom right while the others keep the similar shape but with different pinching. This phenomenon demonstrated the value of ξ_{10} has a maximum limit that is around 0.99. Although the variation of ξ_{10} brings the change of energy dissipation of BWBN model, as the figure 36 exhibited, the difference among each other is too small that can be ignored, which

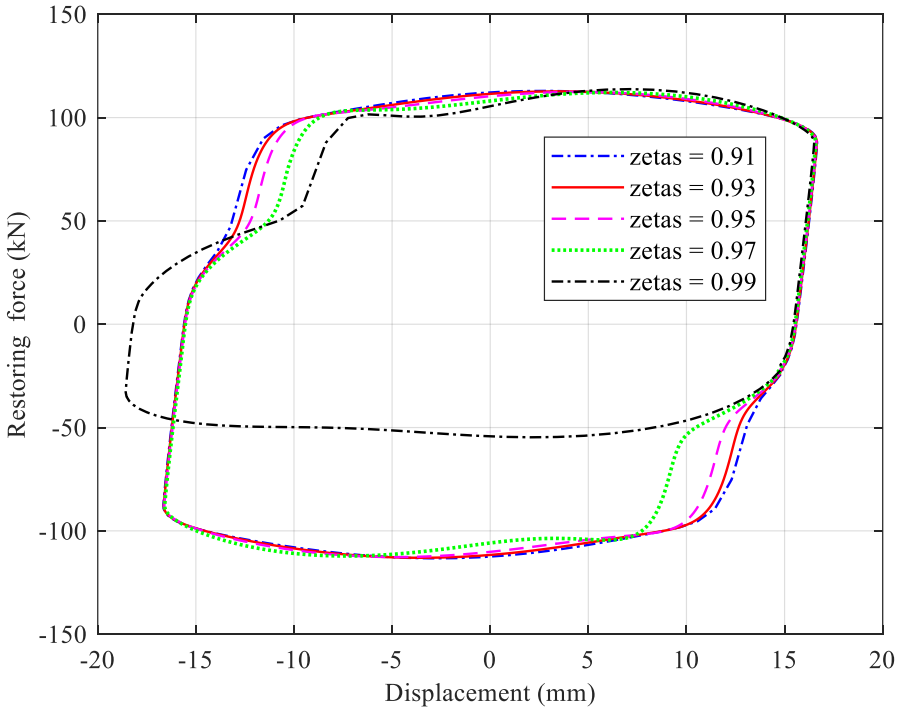

Figure 36. Hysteretic response with different ξ_{10}

confirmed ξ_{10} is just a parameter that can adjust the shape of the hysteresis loop of BWBN model without obvious improvement to energy dissipation.

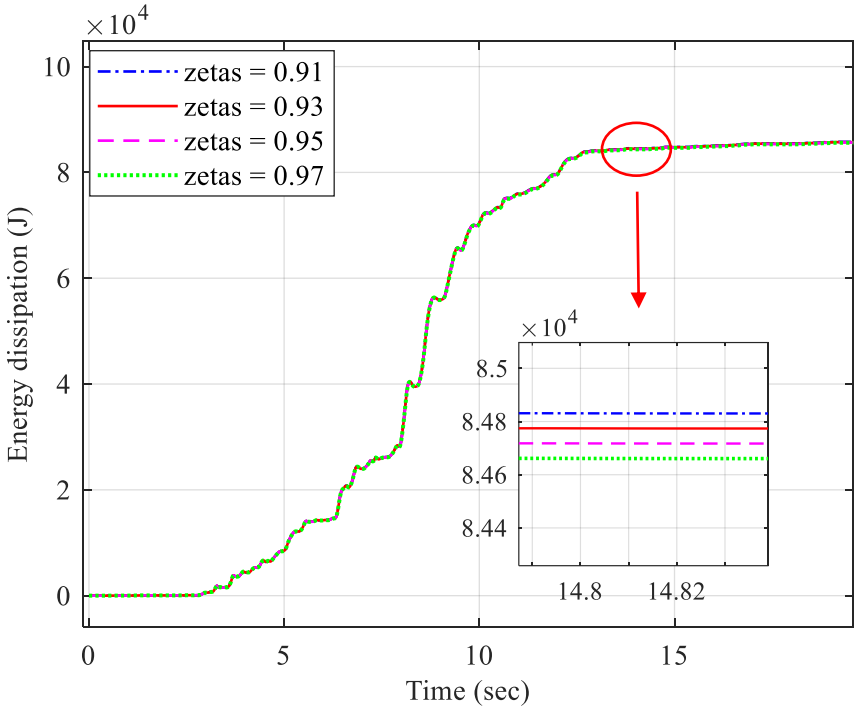

Figure 37. Cumulative energy dissipated by MR-BWBN

Chapter 6. Discussion and Conclusion

Steel moment-resisting frames (SMF) have been in use extensively in high-rise buildings, for the superior earthquake-resisting capability, and the advantage that can provide wide and open spaces without structural walls blocking the view. However, after the Northridge earthquake of 1994, the shortcomings of SMF were exposed. The severely damaged steel building leads to heavy casualties and massive property loss that reach billions of dollars. Since then, FEMA initiated the SAC steel project to investigate the failures of the damaged steel building and suggest preventive measures to reinforce the existing buildings. The result of the investigation reported that the main issue is the brittle connection damage of SMF. Because of the high stiffness, the structural components could not help releasing energy via plastic deformation, in addition to the stress concentration at the beam-column connections resulted from welding defects, the SMF was severely damaged due to the brittle fractures at the joints between the beam flanges and columns flanges. Therefore, except for the design of the plastic hinge zone at beam end, a variety of energy dissipation devices were developed to solve the issue. The magnetorheological (MR) fluid damper stands out for its endurance, instant response, and adjustable damping force, meanwhile, various mathematical models were proposed to describe the behaviors of MR damper. This paper compared two different mathematical models of MR damper and a conventional viscoelastic damper model, to evaluate the performance of MR damper in seismic resistance.

A FEM-based software OpenSees carried out all the analyses, including modal analysis, pushover analysis, harmonic analysis, and transient analysis. Because the one-bay multi-story structure can be idealized as an SDOF system, a one-bay, one-story moment

frame was selected as the carrier for MR damper models. To make sure the accuracy of modeling in OpenSees, the simple MF went through modal analysis and pushover analysis, the results were proved that the modeling of MF in OpenSees can be used in the subsequential analyses with dampers, after comparing the results with the hand calculation and the simulation in ETABS. The two mathematical models to describe the behaviors of MR damper, are the MR-BW and MR-BWBN model. The MR-BW model consists of a Bouc-wen element, a linear spring, and a viscous dashpot, which are connected in parallel. The MR-BWBN model has a BWBN element with a dashpot working in parallel. The modeling of the viscoelastic damper is based on the Kelvin-Voigt model. They were installed in the diagonal bracing of MF, respectively. To avoid the distinction brought by the different stiffness and damping, all the damper models have the identical elastic stiffness and damping coefficient, hence, all the test cases with damper applied, have the same elastic deformation.

The result of the modal analysis shows that all the test cases had identical natural frequencies if they have the same stiffness and damping. In addition, the structural natural frequency can be up to 20.8% higher than a simple MF when the stiffness of the additional damper reaches 14 $kN.mm^{-1}$. The results of harmonic analyses were almost overlapped. The peak response was at the point when exciting frequency approached the natural frequencies of structures.

Transient analyses are the focus of this report. A SAC prescribed loading was applied to the roof level where the lumped mass located in the form of lateral displacement, and the foundation as ground acceleration, respectively. Under the same transverse loading, the area enclosed in the stress-strain curve of MR-BWBN was the smallest among

the others, which demonstrated the capability of MR-BWBN for controlling plastic deformation is better than the others, and this conclusion was verified by the results of the maximum lateral displacement. In addition, the MR-BWBN had higher maximum lateral displacement than the MR-BW and VE when subjected to a smaller amplitude of the ground acceleration, but lower if subjected to the larger amplitude of the ground motion. After the cyclic loading tests, transient analyses were performed using the scaled seismic records of the Northridge earthquake. By comparison, the maximum drift ratios of MR-BWBN were the lowest when subjected to the rare and mega earthquake. The cumulative energy dissipated by MR-BWBN is less than MR-BW by 5.9% when subjected to the basic level earthquake, but higher than MR-BW by 6.42% under the rare level earthquake, and 7.6% under the mega earthquake. It can be concluded that the MR-BWBN is more suitable for the zone that mega-earthquake may happen. These phenomena may attribute to the extra energy dissipation through degrading hysteretic taking the form of deteriorated stiffness and strength, which is characterized as pinching. The parametric study shows how the parameters of pinching inducing function, k_e, c_0, and ξ_{10}, whose values increased as the input current went up, work on the MR-BWBN model.

Although the performance of MR-BWBN shows the potential for seismic resistance as a damper, there are still a lot of improvements waiting to be done before the MR fluid damper systems of the industrial scale. As the material properties of MR fluid can be adjusted by the input current, we can explore the response of MR dampers to the different control systems, and then improve the performance of MR dampers. Furthermore, considering the influence of matrix material on the properties of MR damper, finding the appropriated material is also significant.

References

[1] B. S. Taranath, *Earthquake Effects on Buildings*. 2016.

[2] M. E. A. Budimir, P. M. Atkinson, and H. G. Lewis, "Seismically induced landslide hazard and exposure modelling in Southern California based on the 1994 Northridge, California earthquake event," *Landslides*, vol. 12, no. 5, pp. 895–910, 2015, doi: 10.1007/s10346-014-0531-8.

[3] D. J. Wald, T. H. Heaton, and K. W. Hudnut, "The slip history of the 1994 Northridge, California, earthquake determined from strong-motion, teleseismic, GPS, and leveling data," *Bull. Seismol. Soc. Am.*, vol. 86, no. 1 SUPPL. B, pp. 49–70, 1996.

[4] K. J. Tierney, "Business impacts of the Northridge earthquake," *J. Contingencies Cris. Manag.*, vol. 5, no. 2, pp. 87–97, 1997, doi: 10.1111/1468-5973.00040.

[5] S. A. Mahin, "Lessons from damage to steel buildings during the Northridge earthquake," *Eng. Struct.*, vol. 20, no. 4–6, pp. 261–270, 1998, doi: 10.1016/S0141-0296(97)00032-1.

[6] F. FEMA, "Recommended seismic design criteria for new steel moment-frame buildings," *FEMA-350*, 2000.

[7] P. Uriz and A. S. Whittaker, "Retrofit of pre-northridge steel moment-resisting frames using fluid viscous dampers," *Struct. Des. Tall Build.*, vol. 10, no. 5, pp. 371–390, 2001, doi: 10.1002/tal.199.

[8] K. A. Porter and K. Cobeen, "Informing a retrofit ordinance: A soft-story case study," in *Structures Congress 2012 - Proceedings of the 2012 Structures Congress*, 2012, pp. 1802–1813.

[9] E. C. Fischer, K. Porter, and E. J. Sutley, “Community Resilience through Mandatory Retrofit Ordinances,” *Struct. Mag.*, pp. 20–23, 2019.

[10] W. Y. Kam, S. Pampanin, and D. Bull, “Experimental Validation of Selective Weakening Approach for the Seismic Retrofit of Exterior Beam-Column Joints,” *2009 NZSEE Conf.*, no. 32, pp. 32–40, 2009.

[11] R. L. Reid, “Seismic Success,” *Civ. Eng. Mag. Arch.*, vol. 90, no. 1, pp. 44–49, 2020, doi: 10.1061/ciegag.0001447.

[12] M. D. Symans *et al.*, “Energy Dissipation Systems for Seismic Applications: Current Practice and Recent Developments,” *J. Struct. Eng.*, vol. 134, no. 1, pp. 3–21, 2008, doi: 10.1061/(asce)0733-9445(2008)134:1(3).

[13] C.-M. Uang and V. V Bertero, “Evaluation of seismic energy in structures,” *Earthq. Eng. \& Struct. Dyn.*, vol. 19, no. 1, pp. 77–90, 1990, doi: https://doi.org/10.1002/eqe.4290190108.

[14] T. T. Soong and M. C. Costantinou, *Passive and active structural vibration control in civil engineering*, vol. 345. Springer, 2014.

[15] M. D. Symans and M. C. Constantinou, “Semi-active control systems for seismic protection of structures: A state-of-the-art review,” *Eng. Struct.*, vol. 21, no. 6, pp. 469–487, 1999, doi: 10.1016/S0141-0296(97)00225-3.

[16] F. Casciati, J. Rodellar, and U. Yildirim, “Active and semi-active control of structures-theory and applications: A review of recent advances,” *J. Intell. Mater. Syst. Struct.*, vol. 23, no. 11, pp. 1181–1195, 2012, doi: 10.1177/1045389X12445029.

[17] H. Tandoh, Y. Cao, and A. Awoyomi, “Smith predictor for slug control with large valve

stroke time," in *27th European Symposium on Computer Aided Process Engineering*, vol. 40, A. Espuña, M. Graells, and L. Puigjaner, Eds. Elsevier, 2017, pp. 1531–1536.

[18] B. F. Spencer Jr and S. Nagarajaiah, "State of the art of structural control," *J. Struct. Eng.*, vol. 129, no. 7, pp. 845–856, 2003.

[19] A. Bathaei, M. Ramezani, and A. Ghorbani-Tanha, "Type-1 and Type-2 Fuzzy Logic Control Algorithms for Semi-Active Seismic Vibration Control of the College Urban Bridge Using MR Dampers," *Civ. Eng. Infrastructures J. (Journal Fac. Eng.*, vol. 50, no. 2, pp. 333–351, 2017, doi: 10.7508/ceij.2017.02.008.

[20] J. Wang and G. Meng, "01 Magnetorheological fluid devices principles,characteristics & appls in MEngg.," vol. 215, pp. 165–175, 1948.

[21] M. Zrinyi, "5 - Magnetically responsive polymer gels and elastomers: properties, synthesis and applications," in *Smart Polymers and their Applications*, M. R. Aguilar and J. San Román, Eds. Woodhead Publishing, 2014, pp. 134–165.

[22] Y. Li, J. Li, W. Li, and H. Du, "A state-of-the-art review on magnetorheological elastomer devices," *Smart Mater. Struct.*, vol. 23, no. 12, 2014, doi: 10.1088/0964-1726/23/12/123001.

[23] G. J. Hiemenz, Y. T. Choi, and N. M. Wereley, "Seismic control of civil structures utilizing semi-active MR braces," *Comput. Civ. Infrastruct. Eng.*, vol. 18, no. 1, pp. 31–44, 2003, doi: 10.1111/1467-8667.t01-1-00297.

[24] B. F. Spencer, S. J. Dyke, M. K. Sain, and J. D. Carlson, "Dynamical model of a magnetorheological damper," in *Proceedings of the 1996 12th Conference on Analysis and Computation*, 1996, pp. 361–370.

[25] B. F. Spencer, J. D. Carlson, M. K. Sain, and G. Yang, “On the current status of magnetorheological dampers: seismic protection of full-scale structures,” in *Proceedings of the 1997 American Control Conference (Cat. No.97CH36041)*, Jun. 1997, vol. 1, pp. 458–462 vol.1, doi: 10.1109/ACC.1997.611840.

[26] B. F. Spencer, S. J. Dyke, M. K. Sain, and J. D. Carlson, “Phenomenological Model for Magnetorheological Dampers,” *J. Eng. Mech.*, vol. 123, no. 3, pp. 230–238, 1997, doi: 10.1061/(asce)0733-9399(1997)123:3(230).

[27] S. J. Dyke, B. F. Spencer, M. K. Sain, and J. D. Carlson, “Modeling and control of magnetorheological dampers for seismic response reduction,” *Smart Mater. Struct.*, vol. 5, no. 5, pp. 565–575, 1996, doi: 10.1088/0964-1726/5/5/006.

[28] M. R. Jolly, J. D. Carlson, and B. C. Muñoz, “A model of the behaviour of magnetorheological materials,” *Smart Mater. Struct.*, vol. 5, no. 5, pp. 607–614, 1996, doi: 10.1088/0964-1726/5/5/009.

[29] Y. Yang, Z. D. Xu, Y. W. Xu, and Y. Q. Guo, “Analysis on influence of the magnetorheological fluid microstructure on the mechanical properties of magnetorheological dampers,” *Smart Mater. Struct.*, vol. 29, no. 11, 2020, doi: 10.1088/1361-665X/abadd2.

[30] D. Q. Truong and K. K. Ahn, “MR Fluid Damper and Its Application to Force Sensorless Damping Control System,” in *Smart Actuation and Sensing Systems*, G. Berselli, R. Vertechy, and G. Vassura, Eds. Rijeka: IntechOpen, 2012.

[31] J. Rabinow, “The magnetic fluid clutch,” *Electr. Eng.*, vol. 67, no. 12, p. 1167, 1948.

[32] J. D. Carlson, “What makes a good MR fluid?,” *J. Intell. Mater. Syst. Struct.*, vol. 13, no.

7–8, pp. 431–435, 2002, doi: 10.1106/104538902028221.

[33] A. Farjoud, M. Ahmadian, N. Mahmoodi, X. Zhang, and M. Craft, “Nonlinear modeling and testing of magneto-rheological fluids in low shear rate squeezing flows,” *Smart Mater. Struct.*, vol. 20, no. 8, 2011, doi: 10.1088/0964-1726/20/8/085013.

[34] H. Wang, H. Zheng, Y. Li, and S. Lu, “Mechanical properties of magnetorheological fluids under squeeze-shear mode,” in *Fourth International Symposium on Precision Mechanical Measurements*, 2008, vol. 7130, pp. 607–612, doi: 10.1117/12.819634.

[35] Y. Ding, L. Zhang, H. Zhu, and Z. Li, “Simplified design method for shear-valve magnetorheological dampers,” *Earthq. Eng. Eng. Vib.*, vol. 13, no. 4, pp. 637–652, 2014, doi: 10.1007/s11803-014-0269-2.

[36] A. Lago, D. Trabucco, and A. Wood, “Chapter 5 - Design procedures for tall buildings with dynamic modification devices,” in *Damping Technologies for Tall Buildings*, A. Lago, D. Trabucco, and A. Wood, Eds. Butterworth-Heinemann, 2019, pp. 235–436.

[37] R. Stanway, J. L. Sproston, and N. G. Stevens, “Non-linear modelling of an electro-rheological vibration damper,” *J. Electrostat.*, vol. 20, no. 2, pp. 167–184, 1987, doi: 10.1016/0304-3886(87)90056-8.

[38] Y. Chae, J. Ricles, and R. Sause, “Development of equivalent linear systems for single-degree-of-freedom structures with magneto-rheological dampers for seismic design application,” *J. Intell. Mater. Syst. Struct.*, vol. 28, p. 1045389X1769824, 2017, doi: 10.1177/1045389X17698240.

[39] T. K. Datta, *Seismic Analysis of Structures*. 2010.

[40] S. Mazzoni, F. McKenna, M. H. Scott, and G. L. Fenves, “The OpenSees command

language manual, version 2.0," *Pacific Earthq. Eng. Res. Cent.*, vol. 264, 2007.

[41] A. K. Chopra, "Dynamics of structures. theory and applications to," *Earthq. Eng.*, 2017.

[42] *Seismic Evaluation and Retrofit of Existing Buildings*. 2014.

[43] Y.-K. Wen, "Method for random vibration of hysteretic systems," *J. Eng. Mech. Div.*, vol. 102, no. 2, pp. 249–263, 1976.

[44] T. T. Baber and M. N. Noori, "Modeling general hysteresis behavior and random vibration application," *J. Vib. Acoust. Trans. ASME*, vol. 108, no. 4, pp. 411–420, 1986, doi: 10.1115/1.3269364.

[45] G. R. Peng, W. H. Li, H. Du, H. X. Deng, and G. Alici, "Modelling and identifying the parameters of a magneto-rheological damper with a force-lag phenomenon," *Appl. Math. Model.*, vol. 38, no. 15–16, pp. 3763–3773, 2014, doi: 10.1016/j.apm.2013.12.006.

[46] M. R. Hossain, M. Ashraf, and J. E. Padgett, "Risk-based seismic performance assessment of Yielding Shear Panel Device," *Eng. Struct.*, vol. 56, pp. 1570–1579, 2013, doi: 10.1016/j.engstruct.2013.07.032.

[47] L. B. Eldred, W. P. Baker, and A. N. Palazotto, "Kelvin-Voigt versus fractional derivative model as constitutive relations for viscoelastic materials," *AIAA J.*, vol. 33, no. 3, pp. 547–550, 1995, doi: 10.2514/3.12471.

[48] ATC, "Quantification of building seismic performance factors," *Fema P695*, no. June, p. 421, 2009.

[49] W. E. Gathings, H. Kubagawa, and M. D. Cooper, "A Distinctive Pattern of B Cell Immaturity in Perinatal Humans," *Immunol. Rev.*, vol. 57, no. 1, pp. 107–126, 1981, doi:

10.1111/j.1600-065X.1981.tb00444.x.

[50] L. H. Xu, X. S. Xie, and Z. X. Li, “Seismic performances of magnetorheological flag-shaped damping braced frame structures,” *Smart Mater. Struct.*, vol. 29, no. 7, 2020, doi: 10.1088/1361-665X/ab8c28.

[51] H. H. Lee, *Finite Element Simulations with ANSYS Workbench 17:. SCD Publications*. SDC publications, 2017.

[52] T. Irvine, “Effective Modal Mass and Modal Participation Factors,” *Vibrationdata*, no. 1, pp. 1–36, 2013, [Online]. Available: http://www.vibrationdata.com/tutorials2/ModalMass.pdf.

[53] K. C. Park, “Transient Analysis Methods in Computational Dynamics,” in *Finite Elements*, Springer, 1988, pp. 240–267.

[54] D. T. Pachoumis, E. G. Galoussis, C. N. Kalfas, and A. D. Christitsas, “Reduced beam section moment connections subjected to cyclic loading: Experimental analysis and FEM simulation,” *Eng. Struct.*, vol. 31, no. 1, pp. 216–223, 2009.

[55] C. T. Lachowicz, “Calculation of the elastic–plastic strain energy density under cyclic and random loading,” *Int. J. Fatigue*, vol. 23, no. 7, pp. 643–652, 2001, doi: https://doi.org/10.1016/S0142-1123(00)00102-X.

[56] A. Dominguez, R. Sedaghati, and I. Stiharu, “Modelling the hysteresis phenomenon of magnetorheological dampers,” *Smart Mater. Struct.*, vol. 13, no. 6, pp. 1351–1361, 2004, doi: 10.1088/0964-1726/13/6/008.